

Models of the Knee in the Energy Spectrum of Cosmic Rays

Jörg R. Hörandel

University of Karlsruhe, Institut für Experimentelle Kernphysik, P.O. Box 3640, 76021 Karlsruhe, Germany
<http://www-ik.fzk.de/~joerg>

Preprint arXiv:astro-ph/0402356

Submitted to Astroparticle Physics 21. November 2003; accepted 26. January 2004

Abstract

The origin of the *knee* in the energy spectrum of cosmic rays is an outstanding problem in astroparticle physics. Numerous mechanisms have been proposed to explain the structure in the all-particle spectrum. In the article basic ideas of several models are summarized, including diffusive acceleration of cosmic rays in shock fronts, acceleration via cannonballs, leakage from the Galaxy, interactions with background particles in the interstellar medium, as well as new high-energy interactions in the atmosphere. The calculated energy spectra and mean logarithmic masses are compiled and compared to results from direct and indirect measurements.

Key words: Cosmic rays; Acceleration; Propagation; Energy spectrum; Knee; Mass composition

PACS: 96.40.De, 98.70.Sa

1 Introduction

Cosmic-ray particles — fully ionized atomic nuclei — are the only matter which reaches the earth from outside the solar system and are accessible for direct investigations. The energy of these particles can exceed even 10^{20} eV, but their acceleration mechanisms and the sites of origin are still under discussion. The energy spectrum is of non-thermal origin and follows a power law $dN/dE \propto E^\gamma$ over many orders of magnitude. The spectrum steepens at energies around 4 PeV from a spectral index $\gamma \approx -2.7$ to $\gamma \approx -3.1$. This feature is commonly called the *knee* and its explanation is generally believed to be a corner stone in understanding the origin of cosmic rays, providing answers to one of the key questions of astroparticle physics.

Many approaches have been discussed in the literature to describe the origin, acceleration, and propagation of cosmic rays and several mechanisms have been proposed to explain the *knee*. In this article the basic ideas of theoretical models are briefly mentioned and the resulting energy spectra and mass compositions are described in section 3.

The steeply falling cosmic-ray flux as function of energy requires increasing apertures and exposure times. Presently, above 1 PeV cosmic rays are experimentally accessible in ground-based installations only. These detectors do not measure the primary particles, instead secondary particles are measured, produced in high-energy interactions in the atmosphere, forming an extensive air shower. This

makes the interpretation of the indirect measurements very difficult and the results obtained depend on the understanding of high-energy interactions in the atmosphere. The actual experimental status is briefly discussed in section 2.

2 Experimental results and the *poly-gonato* model

Recently, the results of direct measurements of energy spectra of individual elements and indirect measurements of the all-particle spectrum of cosmic rays have been investigated by the author [1]. It has been shown, that the observed energy spectrum and mass composition can be described consistently in the energy range from 10 GeV up to at least 100 PeV, adopting a phenomenological model, the *poly-gonato* model.

The energy spectra of individual nuclei are assumed to follow power laws with a cut-off at high energies. For the cut-off different approaches have been tried, the cut-off energy has been taken proportional to either the nuclear charge or the nuclear mass of the individual elements. In addition, also a constant cut-off energy has been assumed. Two possibilities for the spectral shape above the cut-off energy have been investigated, a common spectral slope γ_c for all elements and a constant difference $\Delta\gamma$ of the spectral index before and above the cut-off energy.

Individual spectra of elements, as directly measured at the top of the atmosphere for energies below 1 PeV, are extrapolated to high energies and fitted to results from air-shower measurements. For these indirect measurements the individual energy spectra had been normalized to match the all-particle spectrum of direct measurements at 1 PeV. It turned out, that only small energy shifts were necessary, all within the quoted errors — but as a result all air-shower measurements yield consistent all-particle energy spectra.

It turned out that a cut-off proportional to the nuclear charge describes the data best. The modeling of the cut-off behavior seems not to be crucial for the description of the measurements, the two assumptions of a common γ_c and a common $\Delta\gamma$ yield almost the same results. The en-

ergy spectra obtained are hardly distinguishable from each other. In addition, a significant contribution of ultra-heavy elements in the energy region around 10^8 GeV has been found. With the *poly-gonato* model two prominent features in the cosmic-ray spectrum can be explained. The *knee* at 4.5 PeV follows from subsequent cut-offs for individual elements, starting with protons, and the *second knee* at 400 PeV is due to the end of the galactic component.

In the past air shower experiments mostly derived all-particle energy spectra from their measurements. However, recently also results on the energy spectra for groups of elements in the PeV region have been derived from indirect measurements.

The KASCADE group performed systematic studies to evaluate the influence of different hadronic interaction models used in the simulations to interpret the data on the resulting spectra for elemental groups [2, 3, 4, 5, 6]. Two sets of preliminary spectra, derived from the observation of the electromagnetic and muonic air shower components, using CORSIKA [7] with the hadronic interaction models QGSJET and SIBYLL are compiled in Figure 1. In order to compare the results with other measurements and theoretical predictions, the flux of the all-particle spectrum has been normalized to the average measured flux, as obtained by many experiments [1], represented by the solid line in the figure. For the normalization, the energy scale has been slightly adjusted by $\delta_E = -15\%$ for both interaction models used. For comparison, also spectra according to the *poly-gonato* model are given.

As can be seen in the figure, the flux for elemental groups depends on the model used. The KASCADE group emphasizes that at present there are systematic differences between measured and simulated observables, which result in the ambiguities of the spectra for elemental groups. These conclusions apply similarly also to other experiments. A correct deconvolution of energy spectra for elemental groups requires a precise knowledge of the hadronic interactions in the atmosphere. It seems that the interaction models presently used do not describe the measurements with the high precision required.

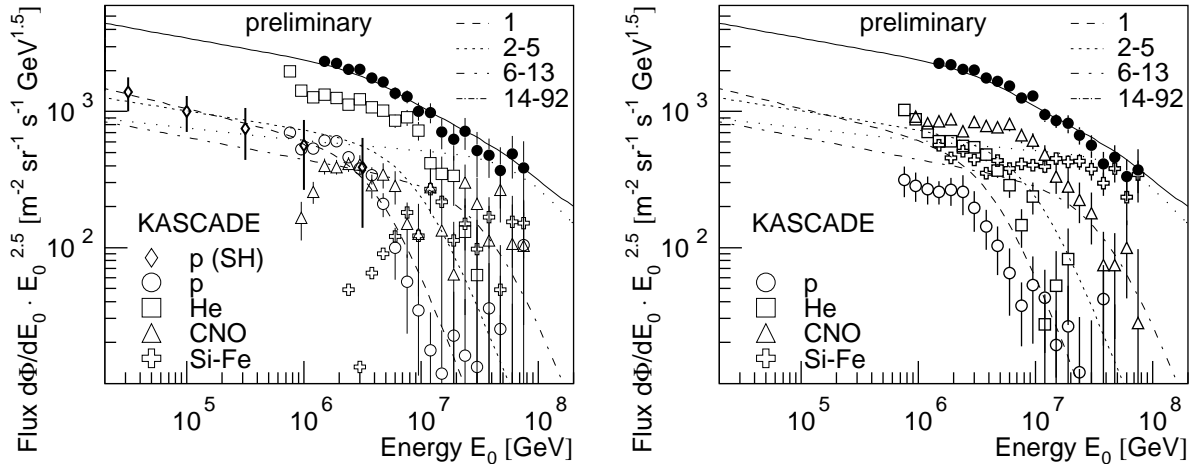


Figure 1: Preliminary energy spectra for groups of elements as obtained by the KASCADE experiment investigating the electromagnetic and muonic components [6], as well as single hadrons [8], using CORSIKA simulations with the hadronic interaction models QGSJET (left-hand side) and SIBYLL (right-hand side) to interpret the data. The energy scale of the data has been readjusted, see text. The all-particle flux is represented by the filled symbols. The solid line gives the average all-particle flux from several experiments [1]. The dashed and dotted lines indicate spectra according to the *poly-gonato* model for elemental groups with nuclear charge numbers as listed.

Nevertheless, analyzing the flux for individual elemental groups, both sets of spectra indicate a rigidity dependent cut-off. While the absolute flux values obtained are different compared to the *poly-gonato* model, the cut-off behavior for the individual groups is very similar to the spectra according to the phenomenological approach. Also presented is the flux of protons obtained from an analysis of unaccompanied hadrons [8], which is found to be compatible with the extrapolations of the direct measurements below the *knee*.

The results of the EAS-TOP experiment are summarized in Figure 2. The proton spectrum as derived from unaccompanied hadrons [9] agrees well with the extrapolation of the direct measurements. The combined analysis of EAS-TOP Čerenkov and MACRO muon data [10] have been normalized ($\delta_E = -15\%$) to the proton+helium flux of direct measurements, otherwise the flux for p+He+CNO would exceed the average measured all-particle spectrum. The results obtained are compatible with the extrapolation of the direct measurements. The spectra derived from the number of electrons and muons (scaled by $\delta_E = -5\%$) are given for two cases

[11, 12]. In the first, the light component consists of protons only and in the second scenario it is a mixture of protons and helium nuclei. The range obtained is indicated by the two sets of points for each mass group.

The HEGRA collaboration derived a sum-spectrum for the proton and helium component as well as an all-particle spectrum [13], as shown in Figure 3. The all-particle spectrum has been normalized to the average measured flux ($\delta_E = -10\%$). Below 1 PeV the flux for protons and helium is lower than the extrapolations of the direct measurements, while at higher energies the data compare well to the *poly-gonato* model.

The figure also reviews the spectra obtained by the Tibet group [14, 15, 16], the all-particle spectrum has been normalized to the average measured spectrum ($\delta_E = -10\%$). The spectra for protons and helium nuclei are below the extrapolations of the direct measurements using single power laws. However, one has to keep in mind that these results are obtained with a very limited number of events observed. As example, the results of 2003 [16] are based on less than 200 registered events. On the other hand,

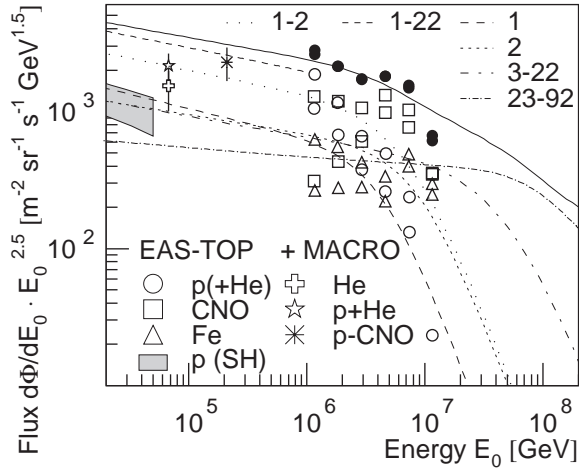


Figure 2: Energy spectra for groups of elements as obtained by the EAS-TOP experiment from the analysis of single hadrons [9], the electromagnetic and muonic components [11, 12], and a combined analysis of Čerenkov light and high-energy muons registered by the MACRO detector [10]. The energy scale of the data has been readjusted, see text. The all-particle flux is represented by the filled symbols, see also caption of Figure 1.

the experiments mentioned previously use data with high statistics, e.g. the KASCADE group uses $O(10^6)$ events for their analysis.

It is worth mentioning that all energy shifts applied have a negative sign, i.e. the energy is overestimated by the hadronic interaction models used to interpret the measured data. A possible explanation for this behavior could be a too large increase of the inelastic cross sections as function of energy, as pointed out in [17].

It should be emphasized that the *poly-gonato* model is based on individual element spectra from direct measurements and the all-particle spectrum from indirect measurements only. The energy spectra for elemental groups derived from air shower measurements as just discussed are not taken into account. Hence, the *poly-gonato* model can be treated as independent result and it is interesting to realize that the predicted spectra are compatible with the deconvoluted spectra from indirect measurements.

However, the present experimental status concerning energy spectra for elemental groups in the PeV region is not yet conclusive. Additional

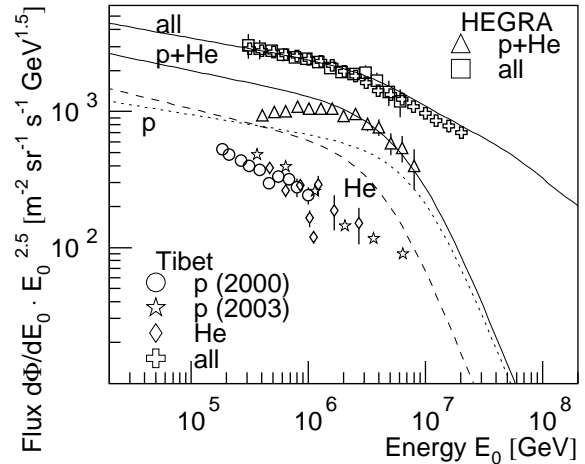


Figure 3: Energy spectra for groups of elements as obtained by the HEGRA [13] and Tibet [14, 15, 16] groups. The energy scale of the data has been readjusted, see text. The solid line gives the average all-particle flux from several experiments [1]. The dashed and dotted lines indicate spectra according to the *poly-gonato* model for protons and helium nuclei.

information from a robust observable like the mean logarithmic mass would be very helpful to evaluate the predictions of various theoretical models of the *knee*. The mean logarithmic mass, defined as $\langle \ln A \rangle = \sum r_i \ln A_i$, with the relative fraction r_i of the element with mass number A_i is an often used quantity to characterize the cosmic-ray mass composition.

In the earlier article [1] experimental $\langle \ln A \rangle$ values have been investigated. A systematic difference has been found in the mean logarithmic mass calculated from experiments measuring particle distributions at ground level and detectors observing the average depth of the shower maximum. A recent investigation showed, that the discrepancy can be reduced, if the logarithmic increase of the inelastic cross-sections in the model QGSJET is lowered and the elasticity of the interactions is increased [17].

Taking the experimental values from experiments measuring particle distributions at ground level [1] and results from experiments observing the average depth of the shower maximum according to an interpretation with a modification of QGSJET (model 3a in [17]), the aver-

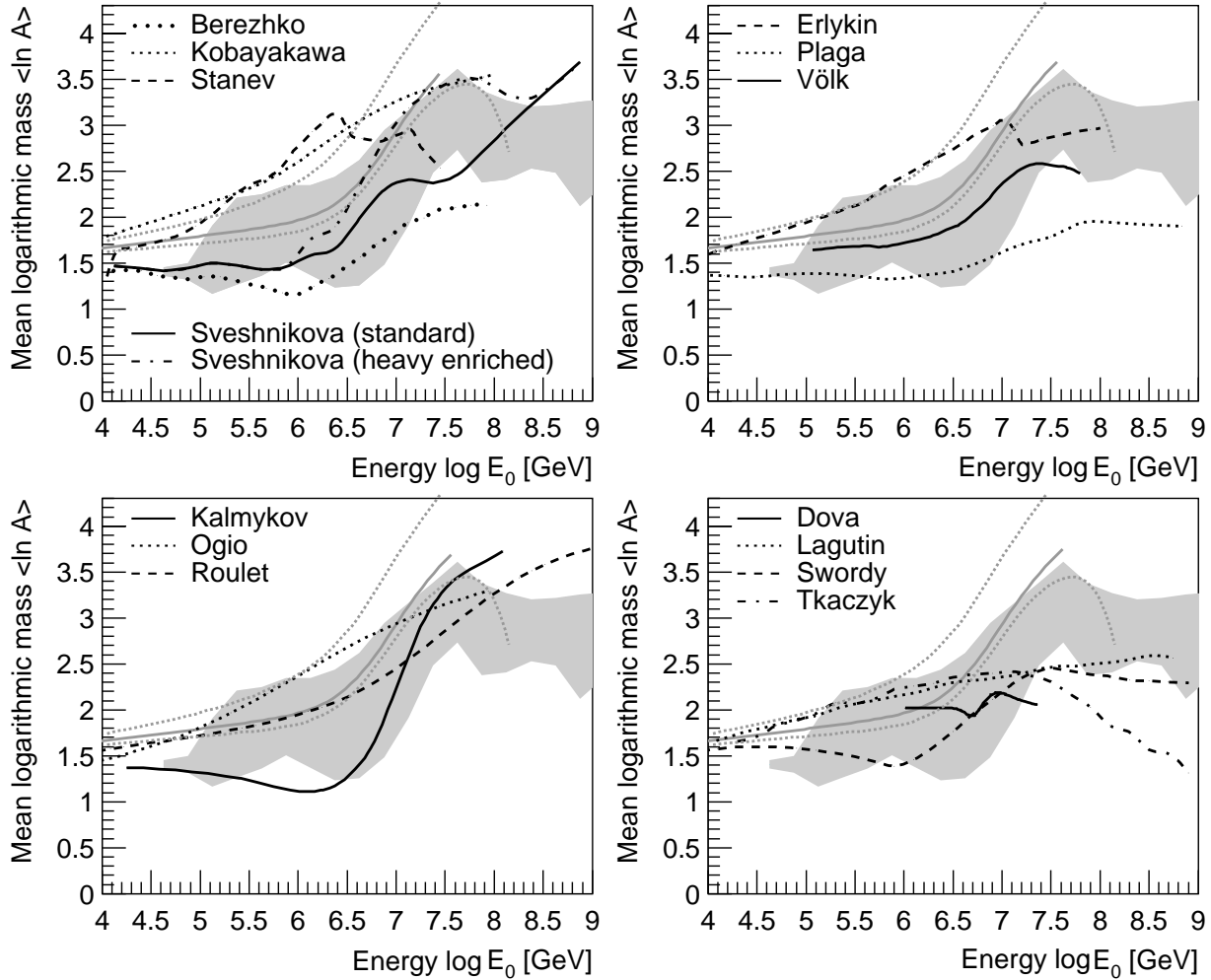


Figure 4: Mean logarithmic mass derived from many experiments (shaded area) compared to $\langle \ln A \rangle$ as obtained with different models. Upper left panel: Acceleration in supernova remnants as described by Berezhko and Ksenofontov [18], Kobayakawa et al. [20], Stanev et al. [19], and Sveshnikova [21]. Upper right panel: Source and acceleration related models by Erlykin and Wolfendale [22], Plaga [24], as well as Völk and Zirakashvili [23]. Lower left panel: Diffusion models by Kalmykov et al. [42], Ogio and Kakimoto [28], as well as Roulet et al. [29]. Lower right panel: Propagation models by Dova et al. [31], Lagutin et al. [26], Swordy [25], and Tkaczyk [30]. In addition, the range of $\langle \ln A \rangle$ for the extrapolation of direct measurements according to the *poly-gonato* model is indicated as dotted grey lines, see text.

age mean logarithmic mass has been calculated. For details on the experiments and references the reader is referred to [1, 17]. The mean value and the variation as function of primary energy are given in Table 1 for reference. The average experimental values are also presented graphically as shaded area in Figure 4 together with the predictions of various models as described below in section 3.

The values calculated with the *poly-gonato*

model are presented in Figure 4 in addition as grey lines. The inclusion of ultra-heavy elements has only a minor effect on $\langle \ln A \rangle$, at 10^8 GeV the values with and without ultra-heavy elements differ only by $\Delta \langle \ln A \rangle \approx 0.2$. The dotted lines depict the systematic errors of the model resulting from the uncertainties of the direct measurements and the errors of the fit parameters of the *poly-gonato* model. In order to include also systematic effects caused by the assump-

Table 1: Average mean logarithmic mass $\langle \ln A \rangle$ as obtained from many experiments as function of primary energy E_0 [GeV]. $\sigma_{\langle \ln A \rangle}$ denotes the variation, not the error of the mean value.

$\log_{10} E_0 [\text{GeV}]$	$\langle \ln A \rangle$	$\sigma_{\langle \ln A \rangle}$
5.12	1.54	0.37
5.38	1.74	0.47
5.62	1.81	0.44
5.88	1.93	0.42
6.12	1.86	0.49
6.38	1.84	0.60
6.62	1.94	0.68
6.88	2.22	0.73
7.12	2.54	0.62
7.38	2.93	0.45
7.62	3.17	0.44
7.88	2.88	0.50
8.12	2.84	0.43
8.38	2.87	0.34
8.62	2.85	0.37
8.88	2.69	0.57

tions made in the model, $\langle \ln A \rangle$ has been calculated for $1 \leq Z \leq 28$ and $1 \leq Z \leq 92$, with a common γ_c and a common $\Delta\gamma$, as well as with and without *ad-hoc* component. The largest and smallest values obtained with these combinations are shown in the figure, representing the total systematic error. The errors are asymmetric, since compared to heavy elements the energy spectra of light elements are specified more precisely by direct measurement.

It should be mentioned that at energies below 1 PeV the indirect observations obtain a lighter mass composition than the direct measurements. The $\langle \ln A \rangle$ range of the latter is bounded by the dotted grey lines.

3 Theoretical models for the *knee*

Proposed explanations in the literature for the *knee* may be divided into four categories. The first three discuss astrophysical reasons, arguing that the *knee* is an intrinsic property of the energy spectrum, while in the last class the authors consider new particle physics processes in the atmosphere. In these theories the *knee* does

not exist in the primary energy spectrum, but is only an effect of observing extensive air showers in the atmosphere:

1) Models in the first category relate the *knee* to the acceleration process. The standard approach of particle acceleration in shock fronts from supernova explosions and several extensions are discussed in the models by Berezhko and Ksenofontov [18], Stanev et al. [19], Kobayakawa et al. [20], and Sveshnikova [21]. The maximum energy attained is taken to be responsible for the *knee*. Also source related is the proposal of Erlykin and Wolfendale [22], namely that a nearby supernova as a single source of cosmic rays causes the structure in the energy spectrum. Völk and Zirakashvili [23] consider reacceleration by spiral shocks in the galactic wind. Plaga [24] proposes cosmic rays being accelerated by cannon balls ejected into the galactic halo.

2) Models of the second category connect the *knee* with leakage of cosmic rays from the Galaxy. Swordy [25] combines diffusive shock acceleration with an energy dependent propagation pathlength in a Leaky Box model. In the models by Lagutin et al. [26], Ptuskin et al. [27], Ogio and Kakimoto [28], as well as Roulet et al. [29] the *knee* follows from diffusive propagation of cosmic-ray particles through the Galaxy.

3) Interactions of cosmic rays with background particles in the Galaxy are considered as origin for the *knee* in the third category. Tkaczyk [30] suggests diffusive propagation in combination with photo-disintegration. Interactions of cosmic rays with background photons are proposed by Dova et al. [31]. Candia et al. [32] discuss the interaction of cosmic rays with the neutrino background.

4) A last class of theories accounts the air shower development in the atmosphere for the *knee*. The basic idea is that a new type of interaction transfers energy to a component not observable (or not yet observed) in air shower experiments. The threshold for these new interactions is in the *knee* region, above the energy of today's collider experiments. In the model by Kazanas and Nicolaidis the energy is transferred into techni-hadrons, lightest supersymmetric particles [33], and gravitons [34].

In the original publications different representations for the theoretical spectra are used, including different sets of mass groups and energy multipliers for the flux values. In order to provide an overview on the predicted spectra and to allow an easy comparison, all results are presented in a standard format with the ordinate being multiplied by $E^{2.5}$. The energy spectra are given for the following five mass groups: protons ($Z=1$), helium ($Z=2$), intermediate: lithium – fluorine ($Z=3-9$), heavy: neon – titanium ($Z=10-22$), and very heavy: vanadium – uranium ($Z=23-92$).

To provide some orientation for the comparison of different models, in the figures depicting the results of the individual models also calculations according to the *poly-gonato* model are shown. As has been discussed in section 2 these spectra are reasonable approximations of the spectra for elemental groups as derived from air shower measurements.

3.1 Acceleration in supernova remnants

The first four models deal with different variations of diffusive shock acceleration of cosmic rays in shock fronts. The maximum energy reached in this process is related to the *knee* in the energy spectrum. The calculations by Berezhko and Ksenofontov [18] are based on the nonlinear kinetic theory of cosmic-ray acceleration in supernova remnants. The mechanical energy released in a supernova explosion is found in the kinetic energy of the expanding shell of ejected matter. The cosmic-ray acceleration is a very efficient process and more than 20% of this energy is transferred to ionized particles. The acceleration is achieved in the following way: The diffusive propagation of high-energy particles allows them to cross the shock front many times and every pair of consecutive crossings of the shock front increases the energy of the particles. In linear approximation this process generates a power-law momentum spectrum at a planar shock front. Due to the high acceleration efficiency and the hardness of the spectrum the structure of the shock wave is modified by the reciprocal influence of cosmic rays on the medium and, in consequence, the cosmic-ray spectrum is

altered.

The particles need some minimum velocity in order to cross the shock front. This velocity determines the injection rate of particles into the acceleration regime. Superthermal particles can efficiently be injected and accelerated with high efficiency. The injection efficiency is expected to be an increasing function of the mass to charge ratio (A/Z) of the nucleus considered, i.e. heavy elements are accelerated more efficiently and obtain a harder spectrum. The energy limit of cosmic rays accelerated in supernova remnants is controlled by geometrical factors of the expanding shock front. Taking into account preacceleration in the wind of the predecessor star maximum energies up to $Z \cdot 10^{15}$ eV can be achieved. In regions modified by the presupernova wind the magnetic fields are larger than in the unperturbed interstellar medium. For the calculations the density of elements heavier than hydrogen in the interstellar medium is assumed to be proportional to the relative abundance of elements in the local, solar region of the Galaxy. The expansion of the shock wave into a hot interstellar medium, which is assumed to be significantly modified by presupernova winds of type Ib and type II supernovae, with a magnetic field $B_0 = 12 \mu\text{G}$ has been taken into account with an injection rate $\eta = 5 \cdot 10^{-4}$.

The resulting energy spectra for five elemental groups are plotted in Figure 5 (symbols). The *knee* in the all-particle spectrum is due to the charge dependence of the maximum energy achieved in the acceleration process. The proton component exhibits a *knee* at 1 PeV with a relatively small change of the spectral index which keeps the protons to be the dominant component up to 10^8 GeV. Elemental spectra according to the *poly-gonato* model are represented by the lines. They show a steeper decrease of the flux above the *knee* for all elements. Below 1 PeV the spectra for He and the CNO-group of the model by Berezhko & Ksenofontov agree with the *poly-gonato* model, but the heavy elements are suppressed in favor of the protons. On the other hand, the all-particle spectra (solid line and filled dots) are well compatible in shape and absolute normalization.

The mean logarithmic mass has been calcu-

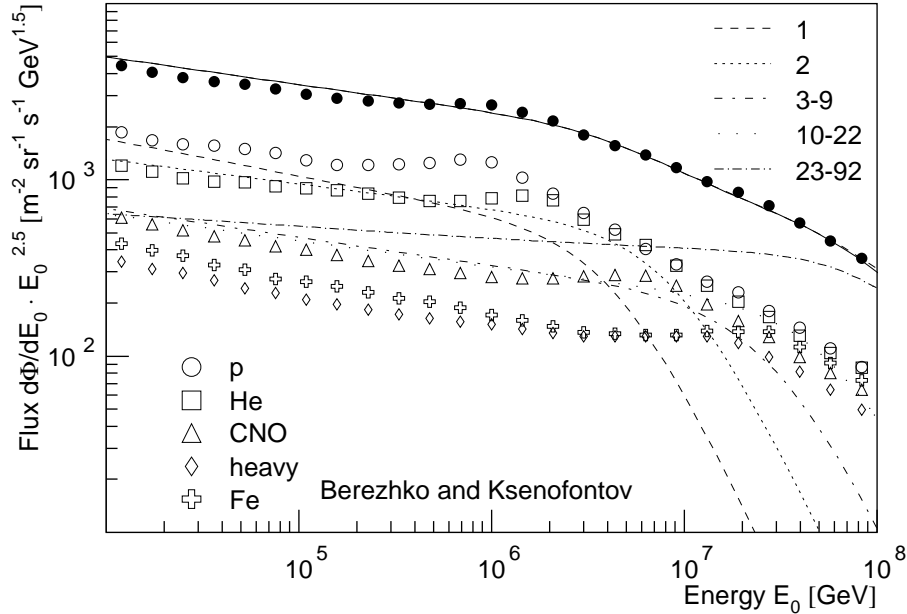


Figure 5: Energy spectra for five groups of elements according to the model by Berezhko & Ksenofontov [18] (open symbols) and the *poly-gonato* model (dashed and dotted lines), the numbers indicate the range of nuclear charge for each group. Filled points and the full line represent the all-particle spectra.

lated using the five mass groups, the result is shown in Figure 4 as function of energy¹. The values exhibit a slight decrease up to about 10^6 GeV to a minimum value around $\langle \ln A \rangle = 1.2$. At higher energies $\langle \ln A \rangle$ increases and reaches $\langle \ln A \rangle = 2.1$ at 10^8 GeV. The rise of $\langle \ln A \rangle$ beyond the *knee* is relatively modest for the model in question, mainly caused by the moderate flux decrease beyond the individual *knees*. In the whole energy range the $\langle \ln A \rangle$ values are at the lower edge or even below the range of measured values.

3.2 Acceleration by supernova shocks

A threefold origin of energetic cosmic rays is proposed by Stanev, Biermann, and Gaisser [19]. In their model particles are accelerated at three different main sites [35]:

1) The explosions of normal supernovae into an approximately homogeneous interstellar medium drive blast waves which can accelerate protons to about 10^5 GeV. Particles are accelerated continuously during the expansion of the spherical shock-wave, with the highest particle

energy reached at the end of the Sedov phase.

2) Explosions of stars into their former stellar wind, like that of Wolf Rayet stars, accelerate particles to higher energies. The maximum energy attained depends linearly on the magnetic field and maximum energies $E_{max} = 9 \cdot 10^7$ GeV for protons and $E_{max} = 3 \cdot 10^9$ GeV for iron nuclei are reached.

3) For energies exceeding 10^8 GeV an extragalactic component is introduced by the authors. The hot spots of Fanaroff Riley class II radio galaxies are assumed to produce particles with energies up to 10^{11} GeV.

In this model the main fraction of galactic cosmic rays above about 10 TeV are assumed to be accelerated by shocks that travel down a steady stellar wind with a Parker spiral structure for the magnetic field. Like in other first order Fermi theories the basic idea for the energy gain is the cyclic crossing of the shock wave from upstream to downstream and back. In most regions the shock normal is perpendicular to the magnetic field. But in small regions around the poles (about 1% of 4π sr) the direction of the propagation of the shock is parallel to the magnetic field which yields harder spectra

¹Only $\langle A \rangle$ versus energy is given in the original article.

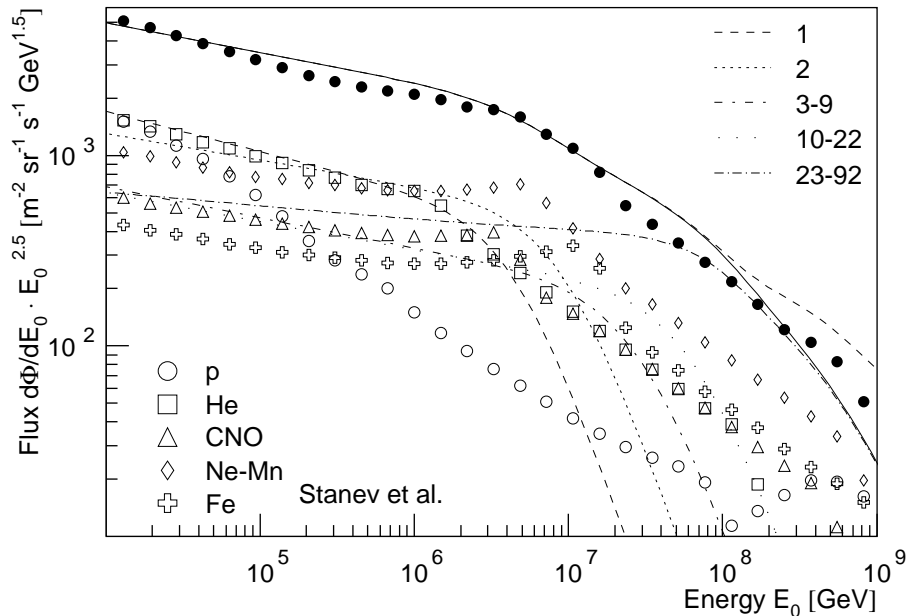


Figure 6: Energy spectra for five groups of elements according to the model by Stanev, Biermann, and Gaisser [19] (open symbols) and the *poly-gonato* model (dashed and dotted lines). The numbers indicate the range of nuclear charge for the elemental groups. Filled points show the sum spectrum for all groups according to the theoretical calculations. The sum spectrum for all elements according to the *poly-gonato* model is represented by a solid line, above 10^8 GeV a dashed line represents the average experimental flux spectrum (see [1]).

for the accelerated particles. The combination of the polar cap with the rest of the stellar hemisphere might lead to a situation where up to about 10^4 GeV the entire hemisphere excluding the polar cap dominates, while from 10^4 GeV up to the *knee* the polar cap begins to contribute appreciably. At *knee* energies the polar cap component contributes equally to the remainder of the 4π sr solid angle. This fact is essentially to describe a sharp bend in the all-particle spectrum as it has been observed by some experiments, e.g. Akeno [36]. The logical consequence of the model is that the chemical composition at the *knee* changes in a way, that the gyroradii of the particles at the spectral break are identical. This implies that the fluxes of different nuclei break off according to their charge Z .

Taking the chemical composition as measured directly by experiments up to 100 TeV energies, Stanev et al. fit the shower size spectra obtained by the Akeno experiment for different zenith angles and derive primary energy spectra for groups of elements. The spectra ob-

tained for five mass groups are reproduced in Figure 6. The proton flux starts to deviate from a power law at 10^4 GeV caused by the energy limit reached for the Sedov phase expansions in the interstellar medium and the flux decreases up to 10^8 GeV. The increase of the proton flux above this energy is caused by the extragalactic component introduced. Elements heavier than hydrogen exhibit a sharp, rigidity dependent bend.

The relative distinct structure of the *knee* is due to the contribution of the polar cap component. Beyond the *knee* the calculated spectra are flatter as compared to the *poly-gonato* model and the contribution of light elements is larger. The sharp *knees* for the individual element spectra result in a pronounced structure in the all-particle spectrum. The model has been tuned to describe the sharp *knee* seen by early experiments like MSU and Akeno. Recent measurements yield a smoother transition at the *knee*, see e.g. Figure 15 in [1]. A fit to the more recent data would probably result in a smaller contri-

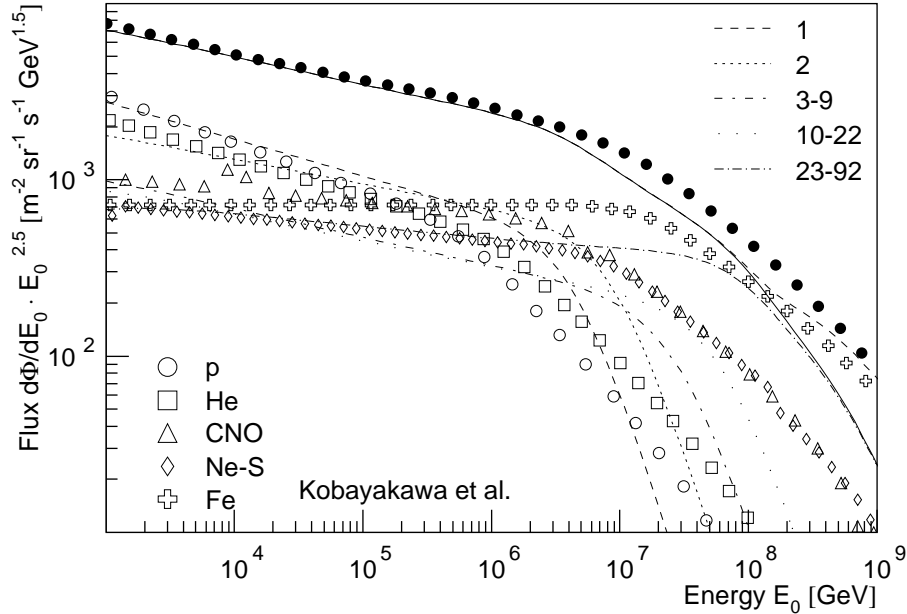


Figure 7: Energy spectra for groups of elements for the model by Kobayakawa et al. [20] (symbols) and the *poly-gonato* model (lines), see caption Figure 6.

bution of the polar cap component.

The mean logarithmic mass calculated from the individual element spectra, shown in Figure 4, exhibits an increase up to $\langle \ln A \rangle \approx 3.1$ at an energy $E_0 \approx 10^7$ GeV. The early increase is caused by the early decrease of the proton flux mentioned. The $\langle \ln A \rangle$ values predicted by the model increase faster as function of energy than the observations, but reach their maximum at lower energies and smaller $\langle \ln A \rangle$ values are predicted at the maximum. The first peak is due to the *knees* in the spectra for the heavy elements (Ne and Fe groups) at energies around 10^7 GeV. The second peak and the decreasing $\langle \ln A \rangle$ values are caused by the extragalactic proton component.

3.3 Acceleration by oblique shocks

A slightly modified version of the diffusive acceleration of particles in supernova remnants is considered by Kobayakawa, Sato, and Samura [20]. Standard first order Fermi acceleration in supernova remnants — with the shock normal being perpendicular to the magnetic field lines — is extended for magnetic fields with arbitrary angles to the velocity of the shock front. The ba-

sic idea is that particles are accelerated to larger energies in oblique shocks as compared to parallel shocks.

The ejected material from a supernova explosion expands into the interstellar medium driving a shock wave. The shock acceleration may be effective until the expanding shell sweeps up its own mass of the interstellar medium. The ejected mass ($\approx 10M_\odot$) with large momenta moves out freely at constant velocity during the free expansion phase which is assumed to be in the order of a few hundred years for ejecta expanding at a velocity $\approx 10^8$ cm/s into a medium of an average density ≈ 1 proton/cm³. The shape of the shock front is supposed to be almost spherically symmetric. The directions of the interstellar magnetic field lines will be, over a wide range, nearly at random rather than well aligned. Therefore, it is assumed that the field lines meet the shock front at random angles and the cosines of the angles are distributed uniformly.

The injection efficiency into the acceleration regime is investigated as function of the angle between the magnetic fields and the normal of the shock front. It is found that the injection efficiency decreases drastically as the shock obliq-

uity increases. The simple relation for the efficiency $\epsilon(\eta) = \eta$ is assumed, η being the cosine of the angle between the magnetic field and the expansion direction of the shock front. On the other hand, the obliquity makes the energy spectrum harder, particles are accelerated more efficiently.

For oblique shocks, reflection at the shock front is more important than diffusion in downstream regions, so that a more rapid acceleration can occur than at parallel shocks. The maximum energies of accelerated particles can be two or even three orders of magnitude larger in the case of a quasi-perpendicular shock than in a parallel one. The maximum energy per particle reached during the acceleration process is mainly limited by the finite lifetime of the supernova blast wave. In the article a rigidity dependent maximum energy

$$E_{max} \propto Z \cdot 2.5 \cdot 10^{16} \text{ eV} \cdot \frac{B}{30 \mu\text{G}} \cdot \frac{u}{10^7 \text{ m/s}} \cdot f(\eta) \quad (1)$$

is derived, with the speed of the shock wave u , the upstream magnetic field B — being about ten times larger than conventionally estimated —, and $f(\eta)$ being an angle dependent acceleration efficiency. For parallel, strong shocks ($\eta = 1$) a maximum energy $E_{crit} = Z \cdot 1.25 \cdot 10^{14}$ eV is obtained. This value is exceeded by more than a factor of 1400 for shocks with extreme obliquity.

The authors fit experimental data for several groups of elements. The spectral indices of the power laws as well as the absolute flux are adjusted at 1 TeV. The resulting spectra are extrapolated to high energies as presented in Figure 7. The individual *knees* result from the dependence of the maximum energy reached on the angle between the shock and the magnetic field. The spectra exhibit a rigidity dependent *knee*. A comparison with the *poly-gonato* model exhibits some differences, but the overall agreement is quite good. However, above the *knees* the model yields slopes less steep and overestimates the all-particle flux.

The cut-off behavior of the iron-group is the reason for the strong increase of the mean logarithmic mass as function of energy, as shown in Figure 4. The model predictions exhibit an increase up to $\langle \ln A \rangle \approx 3.5$ at 10^8 GeV, very close

to the maximum of the *poly-gonato* model. The $\langle \ln A \rangle$ values are at the upper border or even above the experimental values in the whole energy range.

3.4 Acceleration by a variety of supernovae

In a recent article Sveshnikova revised the standard approach of acceleration of cosmic rays in shock fronts of supernovae [21]. The new approach to understand acceleration in supernova remnants (SNRs) is based on recent astronomical observations of supernovae [37, 38]. They indicate that core collapse supernovae prove to comprise the most common general class of exploding stars in the universe and they occur in a great variety of flavors. In particular, supernovae have been observed with unusual large expansion velocities, indicating that these objects are hyper-energetic, the so called hypernovae.

The upper limit of acceleration in SNR is determined essentially by the product of the shock radius R_{sk} , shock velocity $V_{sk} = v_{sk}/1000$ km/s, ejected mass M_{ej} , remnant age T_{snr} , and explosion energy $E_{51} = E_{snr}/10^{51}$ erg. All these values are connected to each other and vary from explosion to explosion. The cut-off energy per particle E_{max} [TeV] can be expressed by a simple formula if only the Sedov Phase of SNR expansion is considered [39]

$$\begin{aligned} E_{max} &= 200 \cdot Z \left(\frac{0.3 \cdot B}{3 \mu\text{G}} \right) \left(\frac{n_H}{\text{cm}^3} \right)^{-\frac{1}{3}} \\ &\cdot \left(\frac{E_{snr}}{10^{51} \text{ erg}} \right)^{\frac{1}{3}} \left(\frac{v_{sk}}{10^3 \text{ km/s}} \right)^{\frac{1}{3}} \quad (2) \\ &= Z \cdot E_{max}^0(B, n_H) (E_{51} \cdot V_{sk})^{\frac{1}{3}} \end{aligned}$$

The maximum energy depends on three factors, the charge Z of the nucleus, the properties of the interstellar medium where the SNR is expanding (strength of magnetic field B and density of protons n_H), and on the energy of the explosion as well as the velocity of the shock.

A usual way to increase E_{max} is to enlarge the magnetic field B , see e.g. the approach by Kobayakawa et al. (section 3.3). On the other hand, as consequence of the recent observations also the parameters of the supernova explosion can be varied. This is the basic idea of Sveshnikova, to draw up a scenario in which the

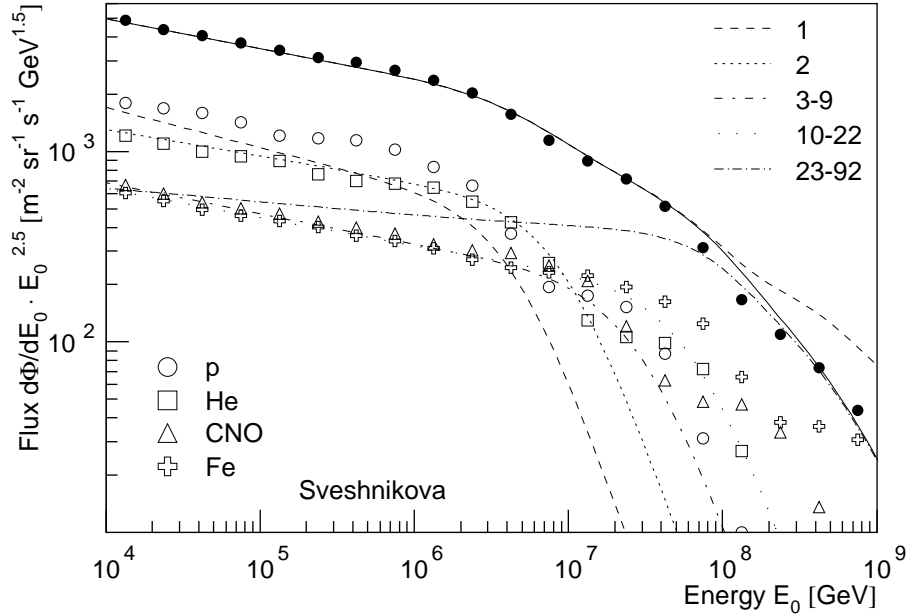


Figure 8: Energy spectra for groups of elements for the model by Sveshnikova [21] (open symbols) and the *poly-gonato* model, see caption of Figure 6.

maximum energy reached in SNR acceleration is in the *knee*-region of the cosmic-ray spectrum (≈ 4 PeV), using only the standard model of cosmic-ray acceleration and the latest data on supernovae explosions.

Based on recent observations the distribution of explosion energies E_{51} and their rates of occurrence in the galaxy are estimated. The spectrum of cosmic rays in each explosion is approximated by a composite power law

$$\Phi(E) = \Phi_0 E^{-\gamma} \quad \text{with} \quad \gamma = \begin{cases} 2.0 & ; 10 \text{ GeV} < E < E_{max}/5 \\ 1.7 & ; E_{max}/5 < E < E_{max} \\ 5.0 & ; E > E_{max}/5 \end{cases} \quad (3)$$

The observed spectrum in the Galaxy is obtained as sum over all different types of supernovae explosions, integrated over the distribution of explosion energies within each supernova group. The mass composition of cosmic rays has been assumed according to direct measurements. As result energy spectra at the source are obtained for groups of elements. In order to take into account propagation effects the spectra given in [21] have been multiplied with $E_0^{-0.65}$, as suggested in the article. The flux has been normalized to the average measured all-particle

spectrum at low energies and the resulting spectra are depicted in Figure 8.

Since the spectra for elemental groups are the result of many supernovae explosions, they can not be described by a simple function with two power laws. Instead, they exhibit a more complicated structure, the cut-off above the individual *knees* is characterized by two subsequent steps, caused by contributions of individual supernovae classes. The the first step for each elemental group occurs at about the same energy as in the *poly-gonato* model. At energies larger than the individual cut-offs, the spectra predicted by Sveshnikova are significantly flatter due to the contribution of very energetic SNRs.

The *knee* in the all-particle spectrum is caused by the cut-off of the proton component. The all-particle spectrum above the *knee* is formed by the sum of coupled steps. The change of the slope beyond the *knee* (in the interval from 3 PeV to $Z_{Fe} \cdot 3$ PeV) is determined by the fraction of iron nuclei in the chemical composition of cosmic rays before the *knee*. The maximal energy of Galactic cosmic rays is determined by iron nuclei generated in the most energetic supernovae (type SNIIn) and corresponds to about 10^9 GeV.

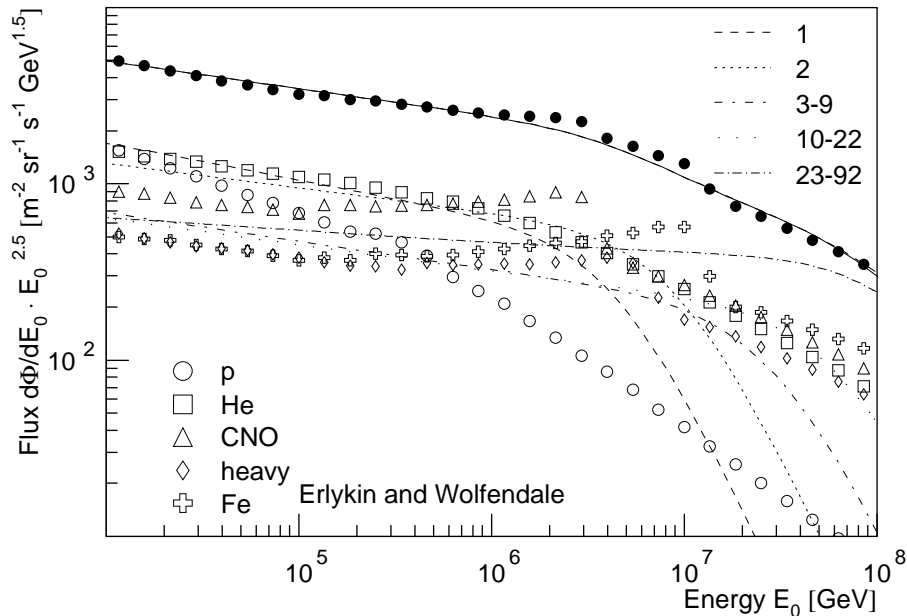


Figure 9: Energy spectra for groups of elements for the model by Erlykin & Wolfendale [22] (open symbols) and the *poly-gonato* model, see caption of Figure 6.

The iron component is clearly dominant at high energies, which leads to a strong increase of the mean logarithmic mass, as can be inferred from Figure 4. A slight structure is visible around 10 PeV, at this energy the light nuclei (protons and helium) are replaced by heavy nuclei as the major component in cosmic rays. The mean logarithmic mass increases to values above $\langle \ln A \rangle = 3.5$ at 10^9 GeV. Additionally, a variant is discussed, where cosmic rays from SNIIn are enriched by heavy nuclei. This results in a heavier mass composition. In the region between 10^7 and 10^8 GeV $\langle \ln A \rangle$ is increased up to 1 unit. The model predictions for both variants are well compatible with the average experimental values. The latter scenario exhibits good agreement with the *poly-gonato* model.

3.5 The single-source model

A different approach is used by Erlykin and Wolfendale [22]. In addition to a background caused by many undefined sources the authors presume a single supernova remnant from a recent and nearby explosion as additional source of cosmic rays. The *knee* in the all-particle spectrum is supposed to have a two-kink struc-

ture related to the cut-offs of oxygen and iron nuclei from the single source. The authors use shower size spectra of the electromagnetic, muonic, hadronic and Čerenkov components of extensive air showers. The shower size spectra are normalized to the same *knee* position. The proposed twofold structure is not visible in all individual shower size spectra considered, it shows up after the normalization and rebinning procedure, combining results from several experiments.

In the publication energy spectra for groups of elements are given for both, the background and the single SNR separately. The sum of both components is shown in Figure 9 for individual element groups. Salient kinks in the spectra of the CNO and Fe groups caused by the single SNR produce a twofold structure in the all-particle spectrum at $3 \cdot 10^6$ GeV and 10^7 GeV. Such a structure is not observable in the averaged all-particle spectrum of the measurements. In the single-source model the *knees* of the elements heavier than helium are much sharper than in the *poly-gonato* model.

The mean logarithmic mass taken from Erlykin and Wolfendale is shown in Figure 4. The early decrease of the proton component results

in a strong increase of $\langle \ln A \rangle$ at the upper border of the observed values. Within the present experimental resolution, the structure at 10^7 GeV can not be resolved.

3.6 Reacceleration in the galactic wind

Reacceleration of cosmic-ray particles in the Galactic wind is discussed by Völk and Zirakashvili [23]. The wind is mainly driven by cosmic rays and hot gas generated in the disk. It reaches supersonic speeds at about 20 kpc above the disk, and is assumed to be very extended (several 100 kpc) before it ends in a termination shock. Due to Galactic rotation the differences in flow speed will lead to strong internal wind compressions, bounded by smooth cosmic-ray shocks. These shocks are assumed to reaccelerate the most energetic particles from the disk by about two orders of magnitude in rigidity, ensuring a continuation of the energy spectrum beyond the *knee* up to the ankle. A fraction of the reaccelerated particles will return to the disk, filling a region around the Galactic plane (several tens of kpc thick) rather uniformly and isotropically.

A maximum energy $E_{max} \approx Z \cdot 10^{17}$ eV is obtained and the authors conclude that the *knee* in the all-particle spectrum cannot be the result of the propagation process, instead it is supposed to be a feature of the source spectrum itself. It is pointed out that it is possible to explain the continuation of the cosmic-ray spectrum above the *knee* up to the ankle in a natural way, by considering the dynamics of the interstellar medium of the Galaxy and its selfconsistent extension into a large-scale halo by the Galactic wind. The authors conclude further that within this picture there is no way to produce higher energy cosmic rays, their sources must be of a different nature.

For the calculations the chemical composition of cosmic rays has been adjusted at $9 \cdot 10^{14}$ eV to KASCADE measurements. The energy spectra derived for four elemental groups as well as the all-particle spectrum are depicted in Figure 10. For the light elements (protons and helium) a *knee*-like structure is clearly visible. For these elemental groups the decrease at high energies is significantly attenuated and the spectra continue at high energies with a spectral slope sim-

ilar to the values below the *knee*. This behavior differs from the *poly-gonato* model with its assumptions on the cut-off behavior, while the all-particle spectra agree well with each other.

The mean logarithmic mass deduced is depicted in Figure 4. In the model iron nuclei are only about a factor of two more abundant than protons at high energies ($E_0 \approx 10^8$ eV). Consequently, only a modest increase of the mean logarithmic mass is obtained with a maximum value $\langle \ln A \rangle_{max} \approx 2.6$. The predictions are well compatible with the average experimental $\langle \ln A \rangle$ values below 10^7 GeV, but may be slightly too low at the highest energies.

3.7 The cannonball model

Within the framework of the cannonball model, originally proposed by Dar and De Rújula [40] to explain gamma-ray bursts, Plaga [24] discusses a mechanism for the acceleration of cosmic-ray hadrons. The author investigates if masses of baryonic plasma ("cannonballs"), ejected in bipolar supernova explosions, could be the universal sources of hadronic galactic cosmic rays. It is assumed, that in each of the symmetric cannonball jets a total energy of 10^{53} erg is ejected. Supernova explosions which eject cannonballs should occur in the Galaxy at rates of $1/(50 \text{ a})$ to $1/(600 \text{ a})$. Less than $1/40$ of the total cannonball-energy has to be converted to the energy of the cosmic-ray particles in order to match the observed cosmic-ray luminosity.

Two scenarios for the acceleration are sketched. The first is based on ultra-relativistic shocks in the interstellar medium and could accelerate cosmic rays up to *knee* energies. The second is based on second order Fermi acceleration inside the cannonballs. For cosmic-ray propagation a diffusion coefficient $D \propto E^{-\alpha}$, with $\alpha = 0.5$, is adopted. No discontinuities in the energy dependence of the diffusion coefficient are assumed, thus the *knee* in the energy spectrum is related to source properties.

The bulk of cosmic rays up to the *knee* is taken to be accelerated at ultra-relativistic shocks driven by cannonballs into the interstellar medium. The accelerated particles are immediately swept up into the plasmoid and remain confined there until it has slowed down to

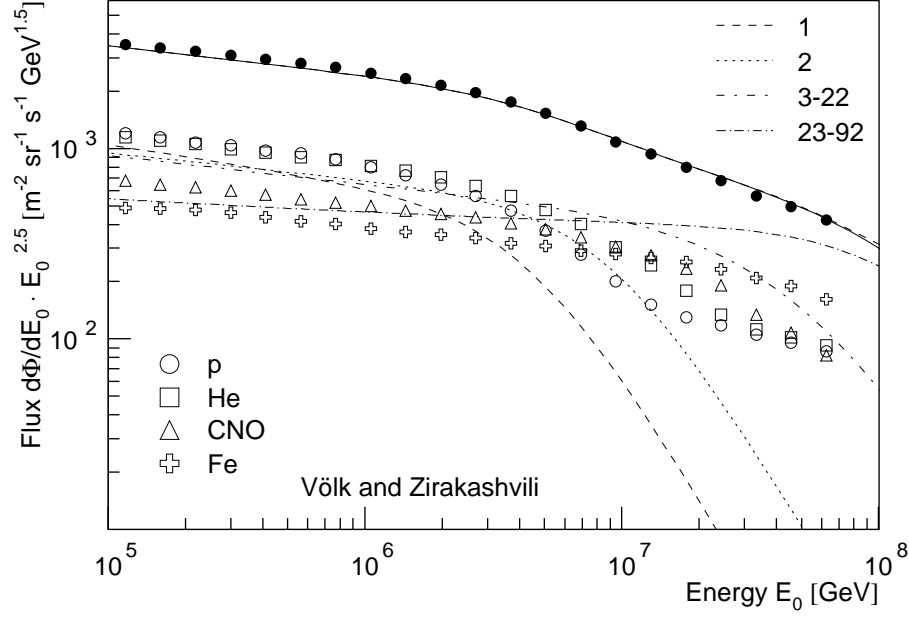


Figure 10: Energy spectra for groups of elements for the model by Völk and Zirakashvili [23] (open symbols) and the *poly-gonato* model, see caption of Figure 6.

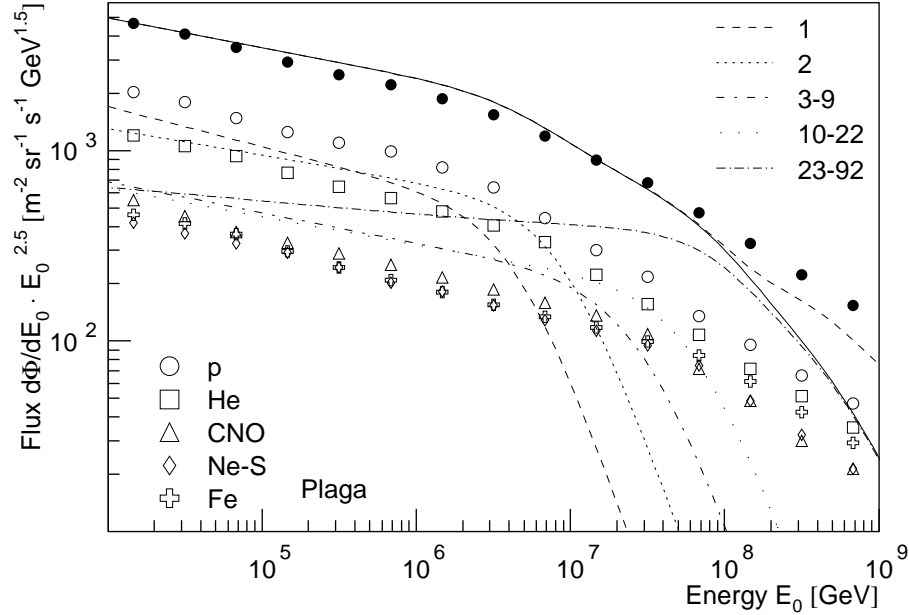


Figure 11: Energy spectra for groups of elements for the model by Plaga [24] (open symbols) and the *poly-gonato* model, see caption of Figure 6.

subrelativistic speeds in the galactic halo. The maximum energy

$$E_{max} = 3 \cdot 10^{15} \text{ eV} \frac{R}{0.02 \text{ pc}} \frac{Z \cdot B}{\mu\text{G}} \frac{\Gamma}{50} \quad (4)$$

that can be reached in this acceleration process

is proportional to the radius of the plasmoid R , to its Lorentz factor Γ , and to the interstellar magnetic field B . Z is the nuclear charge of the accelerated particle. A fraction of particles contained inside the plasmoid escapes by diffusive

processes and determines the observed cosmic-ray luminosity. A power law with an spectral index $\gamma = -2.2$ at the source is obtained below the *knee*.

Even higher energies could be reached inside the cannonballs by further acceleration of contained hadrons in the internal turbulent plasma via second order Fermi mechanisms. Typical acceleration times are in the order of several 10^2 to 10^5 a and energies up to $Z \cdot 10^{20}$ eV could be reached. Again, the particles are diffusively released, their energy spectrum follows a power law with an index $\gamma = -2.5$ at the source.

The energy spectra for groups of elements as obtained by Plaga are presented in Figure 11. The individual spectra exhibit a *knee* proportional to the charge. However, the change in spectral slope is extremely soft. The individual groups decline in the figure almost parallel, without any significant change of the mass composition. The obtained all-particle spectrum is in reasonable agreement with the average measured flux.

In the whole energy range shown, light particles dominate the mass composition. Therefore, only a small increase of the mean logarithmic mass is found above the *knee*, as can be inferred from Figure 4. At an energy of $8 \cdot 10^7$ GeV the maximum value reached is still below 2. The extreme light mass composition predicted by the model seems not to be compatible with the experimental values.

3.8 The minimum-pathlength model

The second class of models discussed describes the propagation of cosmic rays through the interstellar medium. In these scenarios the *knee* is a consequence of leakage of particles from the Galaxy. The calculations by Swordy [25] are based on a Leaky Box model for the cosmic-ray propagation. The spectra of particles accelerated by diffusive shocks are assumed to have the same spectral slope $\gamma = -2.15$ for all elements at the source with a rigidity dependent cut-off at a rigidity $R \approx 10^{15}$ V. Above this cut-off the spectra are assumed to decrease as $dN/dR \propto R^{-3}$. The pathlength λ_e for escape from the Galaxy declines with rigidity but has some minimum value. As function of R it has

been parametrized using the expression

$$\lambda_e = \lambda_0 \left(\frac{R}{R_0} \right)^{-\delta} + \lambda_r \quad (5)$$

with $\lambda_0 = 6$ g/cm², $\delta = 0.6$, and $R_0 = 10$ GV. The value for the minimum pathlength $\lambda_r = 0.013$ g/cm² has been determined by a fit to the measured all-particle spectrum.

Using this set of parameters, the author gives fractional abundances for five elemental groups as function of energy. They are normalized to the mean values of direct measurements in the TeV energy range. Taking the fractional abundances and using the average all-particle spectrum as obtained from many experiments, the energy spectra shown in Figure 12 are calculated. The change of slope for the individual spectra is very smooth in the model by Swordy. Above the *knee* the spectra are significantly flatter as compared to the *poly-gonato* model. The cut-off with R^{-3} seems to be smooth.

The individual spectra show a slight dip just below the individual *knees*. This feature causes the dip in the mean logarithmic mass shown in Figure 4. The $\langle \ln A \rangle$ values have been calculated from the individual spectra shown in Figure 12². They reach a maximum of $\langle \ln A \rangle \approx 2.5$. The modest increase obtained is due to the relative flat spectra above the individual cut-offs, which yields to a mass composition, which is mostly at the lower edge of the experimental values.

3.9 Anomalous diffusion in the Galaxy

Lagutin et al. [26] discuss the *knee* structure as being linked to anomalous diffusion of cosmic rays in the magnetic fields of the Galaxy. In the literature several models are considered to describe the propagation of cosmic rays through the interstellar medium. Frequently, a conception is used in which the propagation process is determined by scattering at magnetic-field inhomogeneities which have small-scale character. They can be considered as a homogeneous Poisson ensemble and the propagation is described by a normal diffusion model, e.g. as discussed by Berezhinsky et al. [41].

²The original publication gives only values for the mean mass.

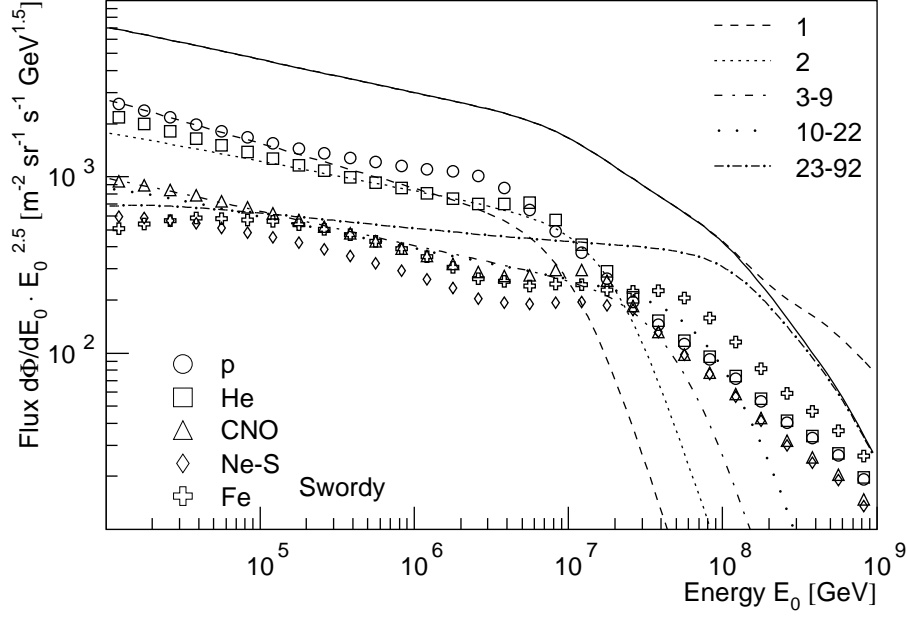


Figure 12: Energy spectra for groups of elements for the model by Swordy [25] (open symbols) and the *poly-gonato* model, see caption of Figure 6.

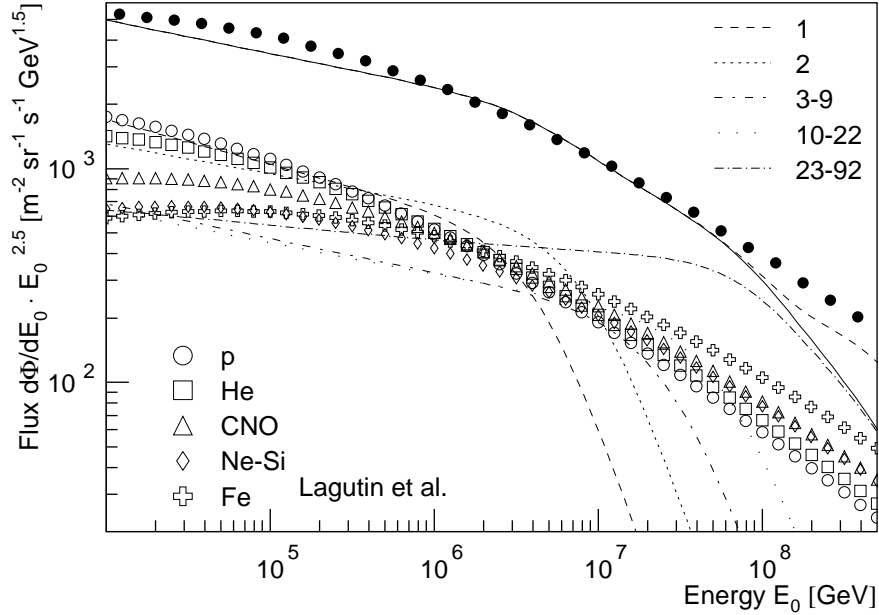


Figure 13: Energy spectra for groups of elements for the model by Lagutin et al. [26] (open symbols) and the *poly-gonato* model, see caption of Figure 6.

Lagutin et al. propose the existence of multiscale structures in the Galaxy, related to filaments, shells, and clouds which are widely spread in the interstellar matter. A rich variety of structures that are created in interacting phases having different properties can be

related to the fundamental property of turbulence. The tool of fractal geometry is used to characterize the interstellar medium and, correspondingly, the magnetic field strength. In such a fractal-like interstellar medium the cosmic-ray propagation can not be described by normal dif-

fusion. Instead, an anomalous diffusion model or superdiffusion is proposed. The anomaly results from large free paths (Lévy flights) of particles between magnetic domains. These paths are distributed according to an inverse power law. Also rest-states of motion in a trap (Lévy waiting times) are investigated.

The diffusion coefficient is assumed to depend on the rigidity of the particles as $D \propto D_0 R^\delta$. D_0 describes the propagation taking into account both, long free paths and the probability to stay in magnetic traps during the propagation. The anomalous diffusion coefficient is evaluated using experimental data on the anisotropy of the cosmic-ray flux in the energy region from 10^3 to 10^4 GeV/nucleus. In the model the spectral index as function of primary energy is derived. The differential flux of all particles is supposed to consist of two components. The first one describes the contribution of nearby sources ($d < 1$ kpc), including 16 supernova remnants, being responsible for the high energy region including the *knee*. The second deals with the bulk of observed cosmic rays with energies from 0.1 GeV to 10 GeV from numerous distant sources ($d > 1$ kpc).

The authors conclude that the *knee* in the primary cosmic-ray spectrum and the observed distinction in the spectral index of protons and other nuclei can be explained by superdiffusion propagation. The energy dependence of particle spectra supports the hypothesis, that nearby supernova bursts are the source of high-energy cosmic rays.

The calculated spectra are shown in Figure 13. Between 1 and 50 PeV absolute flux and shape of the all-particle spectrum are compatible with the measured spectrum, but below and above these energies the calculations overestimate the experimental all-particle flux. The energy spectra for individual elements exhibit a very smooth behavior in the *knee* region, no kink in the spectra is visible and no distinct energy for the *knee* can be specified. At low energies the fluxes of the individual element spectra do not agree with direct measurements and their extrapolation using power laws.

The model is characterized by a very smooth change of the spectral slopes. At the highest

energies above 10^8 GeV the iron-group is only about a factor of two more abundant than protons. The resulting mean logarithmic mass, presented in Figure 4, shows a slow — in the logarithmic plot almost linear — increase as function of energy. At 400 PeV a value of $\langle \ln A \rangle \approx 2.6$ is reached.

3.10 Drift in the global regular magnetic field of the Galaxy

The next three models described (sections 3.10 to 3.12) deal with variations of similar basic ideas. They treat the diffusion of cosmic rays in the Galaxy taking into account the regular magnetic field, a random component, and anti-symmetric diffusion.

Ptuskin et al. [27] demonstrate that a drift (hall diffusion) of particles in the global regular magnetic field of the Galaxy may be responsible for the *knee*. In the galactic halo a random field is assumed to exist simultaneously with the regular magnetic field, which is mainly toroidal and whose value is comparable with the value of the field in the gas disk. Particle diffusion in a magnetically-active medium is described by a tensor. The Hall diffusion, viz. the antisymmetrical part of the cosmic-ray diffusion tensor, is not effective at small energies, but it may control the leakage of cosmic rays out of the Galaxy at energies above 3 PeV. In this way the *knee* in the cosmic-ray power law spectrum is obtained without resorting to any assumptions concerning this feature in the source spectrum or changes in the energy dependence of the diffusion coefficient along the field lines.

The global structure of the regular magnetic field in the Galaxy is very important to describe the propagation of cosmic rays since it determines the orientation of the diffusion tensor. Reliable information on the regular field in the disk is available, revealing that it is predominantly toroidal. Observations indicate that the field lines of the regular field are closed circles and the field changes sign with radial distance after each 3 kpc. It has the same direction above and below the galactic plane.

Only scant information on the magnetic field beyond the galactic disk — i.e. at distances > 500 pc — exists. The orientation of the

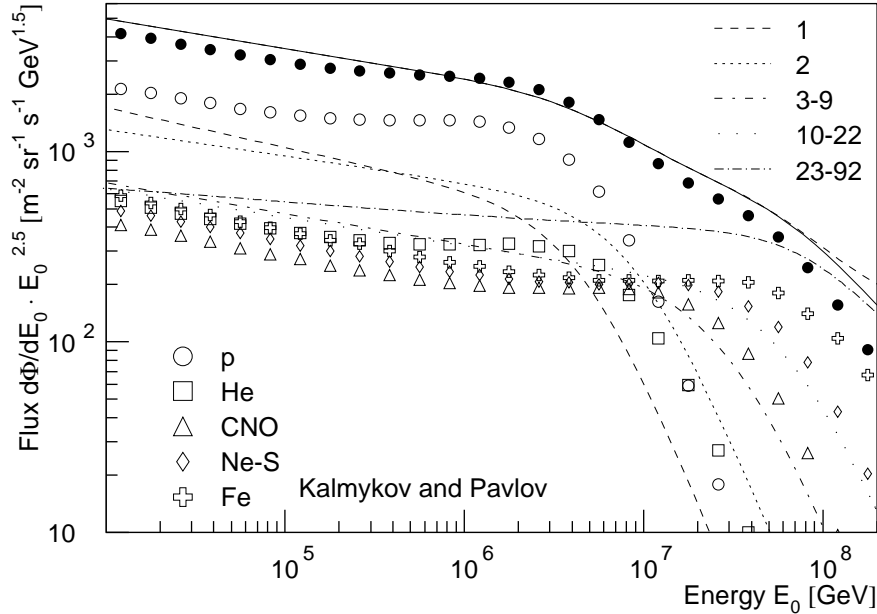


Figure 14: Energy spectra for groups of elements for the model by Ptuskin et al. [27] adapted to experimental data by Kalmykov and Pavlov [42] (symbols) and the *poly-gonato* model, see caption of Figure 6.

regular field in the Galactic halo is not known, but the toroidal components seem to dominate. Ptuskin et al. propose two scenarios, a flat halo model — it is assumed that the propagation region of cosmic rays in the Galaxy has the form of a cylinder and the height of the cylinder is much smaller than its radius — and a large halo model. The latter is supported by radio astronomical data which indicate that our Galaxy has an extended halo with a height of about 10 kpc comparable to the galactic radius ≈ 20 kpc. Numerical calculations of the cosmic-ray propagation in such an environment, assuming a power-law energy spectrum with a constant spectral slope at the source, yield a cosmic ray energy spectrum with a *knee* at 3 PeV.

At energies in the GeV region the Hall diffusion is insignificant and plays a minor part in cosmic-ray leakage from the Galaxy. The Hall diffusion coefficient increases rapidly with energy and begins to dominate the slowly-increasing usual diffusion at ≈ 3 PeV, thus generating the *knee*. Diffusion and drift of different cosmic-ray nuclei at ultrarelativistic energies depend on the energy per unit charge E/Z . Thus, the position of the *knee* for each kind of nucleus

is proportional to Z .

Based on the large halo model Kalmykov and Pavlov [42] have fitted the primary mass composition in order to obtain best agreement with the experimental size spectrum of the MSU array. The resulting energy spectra are shown in Figure 14 for five mass groups as well as the all-particle spectrum. The flux given by the authors has been normalized to the average experimental all-particle flux at 1 PeV. A rigidity dependent cut-off for the individual element spectra is clearly visible.

Except for the absolute normalization, the shape of all elemental groups is very similar for this approach and the *poly-gonato* model. Above 30 PeV the iron group is clearly dominant. This is also reflected by the pronounced increase of the mean logarithmic mass, as can be inferred from Figure 4. The model predicts a very strong increase of $\langle \ln A \rangle$ within a small energy interval. At 10^8 GeV no other model yields such high values of $\langle \ln A \rangle$.

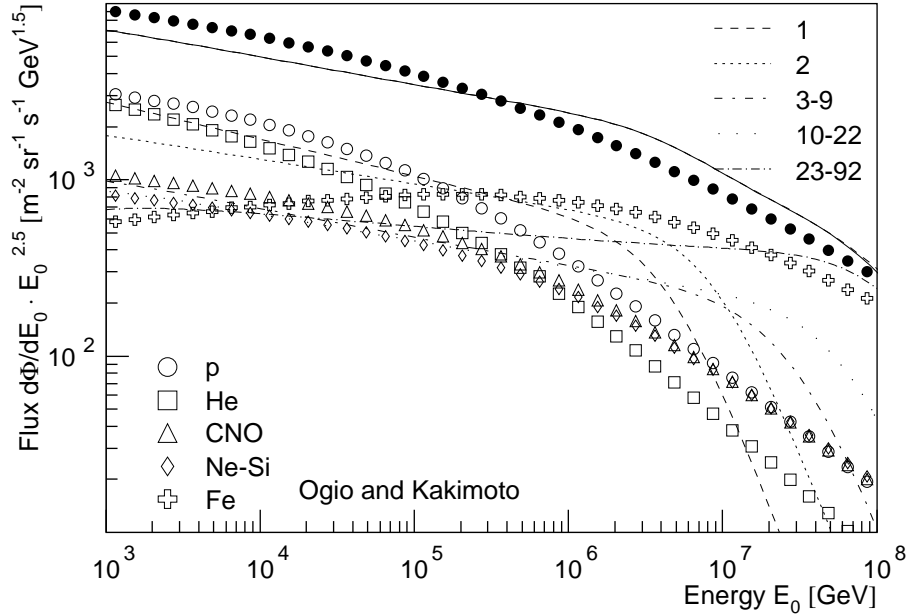


Figure 15: Energy spectra for groups of elements for the model by Ogio and Kakimoto [28] (open symbols) and the *poly-gonato* model, see caption of Figure 6.

3.11 Diffusion in turbulent galactic magnetic fields

Ogio and Kakimoto [28] consider the regular magnetic field in the Galaxy following the direction of the spiral arms. In addition, irregularities of roughly the same strength are supposed to exist. It is assumed that the regular and irregular components have about the same field strength $B \approx 3 \mu\text{G}$ and that both decrease exponentially with a scale height of 1 kpc. The scale length of the irregularities is estimated to about $L_{irr} \approx 50 \text{ pc}$.

The magnetic field lines of the loop and filament structures are open and perpendicular to the galactic disk. In these structures of the disk the confinement of cosmic rays is not strong and the particles are leaking rapidly. The authors assume that the particles leak at this structures with diffusive motions along the magnetic field lines with a diffusion coefficient D_{\parallel} . Additionally, outflows with galactic winds with a velocity $v_g \approx 5 \cdot 10^{-4} \text{ pc/a}$ are anticipated. The leakage of cosmic rays from the Galaxy is described with an one-dimensional advective-diffusion equation

$$\frac{\partial n}{\partial t} + v_g \frac{\partial n}{\partial x} = \frac{\partial}{\partial x} \left(D_{\parallel} \frac{\partial n}{\partial x} \right) + Q \quad (6)$$

The diffusion equation is solved numerically and the residence time τ_R of cosmic-ray particles in the galactic disk is obtained. It is found that τ_R depends on the charge of the particles and that it is smaller for light nuclei. This implies that the average mass of cosmic-ray particles is expected to increase with energy. The relative abundances and the spectral indices for each cosmic-ray component are taken from direct measurements and the all particle spectrum is normalized to direct measurements at 10^{12} eV .

The resulting energy spectra for five groups of elements are presented in Figure 15 together with the all-particle spectrum obtained. The individual components exhibit a relatively smooth *knee* structure, the bends extend over several decades in primary energy. The observed *knee* structure in the all-particle spectrum is not well reproduced by this model. The shape of the average measured energy spectrum (solid line in Figure 15) is described only moderately by the model calculations (filled points).

Since the heavy component clearly dominates above 10^6 GeV , a relative strong increase of the mean logarithmic mass with energy is expected, see Figure 4. At the highest energies ($E_0 \approx 10^8 \text{ GeV}$) values of $\langle \ln A \rangle > 3$ are ob-

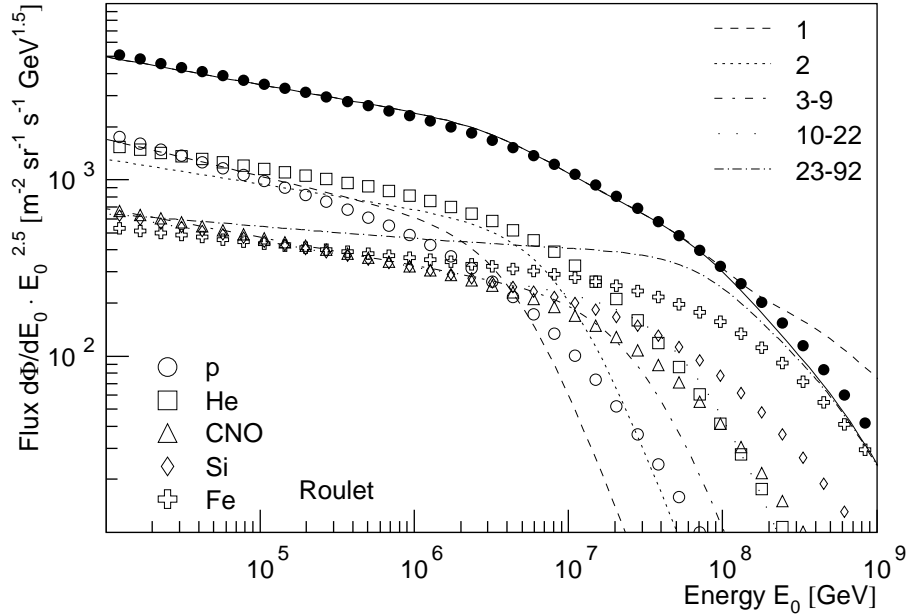


Figure 16: Energy spectra for groups of elements for the model by Roulet [29] and the *poly-gonato* model, see caption of Figure 6.

tained. The increase occurs with an almost constant slope in the logarithmic plot, while the two other diffusion models considered, exhibit a distinct change in the *knee* region.

3.12 Diffusion and drift

Similar to the models discussed previously, Roulet et al. [29] consider the drift and diffusion of cosmic-ray particles in the regular and irregular components of the galactic magnetic field. Again, a three-component structure of the magnetic field is assumed. The regular component is aligned with the spiral arms, reversing its directions between consecutive arms. This field (with strength B_0) will cause particles with charge Z to describe helical trajectories with a Larmor radius $R_L = p/(ZeB_0)$. Secondly, a random component is assumed. This will lead to a random walk and diffusion along the magnetic field direction, characterized by a diffusion coefficient $D_{\parallel} \propto E^m$. The diffusion orthogonal to the regular magnetic field is typically much slower, however the energy dependence of D_{\perp} is similar to D_{\parallel} . The third component is the antisymmetric or Hall diffusion, which is associated with the drift of cosmic rays moving across the regular magnetic field. The antisymmetric

diffusion coefficient is $D_A \approx r_{LC}/3 \propto E$.

In this model, for energies below $Z \cdot E_k$ perpendicular diffusion is the dominant effect, while for larger energies the drifts are responsible for the dominant escape mechanism. The transition between these two regimes is naturally understood from the different energy dependence of the two diffusion coefficients D_{\perp} and D_A . Both coefficients are comparable, $D_{\perp} \approx D_A$, at an energy of the order of $Z \cdot E_k$. This generates a break in the all-particle spectrum.

For the calculations a source spectrum $dQ/dE \propto E^{-\alpha_s}$, with a constant index for all species $\alpha_s = 2.3$ is assumed. Below the *knee*, where transverse turbulent diffusion dominates, the observed spectral index will be $\alpha \approx \alpha_s + 1/3$, while in the drift dominated region above $E \cdot E_k$, $\alpha \approx \alpha_s + 1$ is obtained. This results in a rigidity dependent cut-off for the individual elements, as can be seen in Figure 16. For the calculations, the cosmic-ray composition has been normalized to direct measurements at energies below 10^{14} eV. The change of the slope for individual components $\Delta\alpha \approx 2/3$ is softer than compared to the *poly-gonato* model, where $\Delta\gamma = 2.10$ has been obtained.

Nonetheless, the overall agreement between

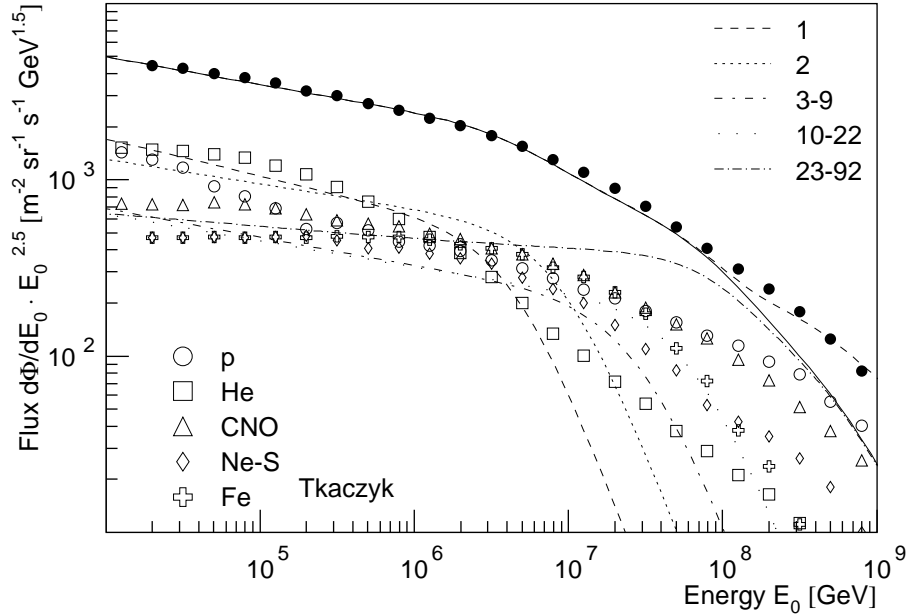


Figure 17: Energy spectra for groups of elements for the model by Tkaczyk [30] (symbols) and the *poly-gonato* model, see caption of Figure 6.

the two approaches is quite good. The iron component is clearly dominant at the highest energies shown. This results in a relatively strong increase of the mean logarithmic mass as function of energy, as can be seen in Figure 4. At 10^9 GeV $\langle \ln A \rangle \approx 3.75$ is reached.

3.13 Photo-disintegration and diffusion

Interactions of cosmic rays with various background particles are considered in the next three models described.

Following an idea suggested by Hillas [43], several authors discuss the possibility of photo-disintegration of nuclei in a dense field of soft photons around discrete galactic sources, e.g. pulsars. Cosmic rays are assumed to be magnetically confined near the source and, therefore, accumulate a large column density on their pass across the photon field. These models are inspired by the indication in some experiments that the mass composition becomes lighter beyond the *knee*. The *knee* is explained by the onset of photodisintegration as well as due to leakage from the Galaxy in the diffusion process in the galactic magnetic field.

Tkaczyk [30] assumes the individual spectra to be described by power laws with a spectral index of $\gamma_p = -2.75$ for protons and $\gamma_x = -2.55$ for all other nuclei up to iron using the abundances observed at 100 TeV by the JACEE experiment. The photon background is taken to have a Planck type distribution with $k_B T = 20$ eV. Three processes of energy loss are taken into account: pair production, pion photo production on nucleons, and photo-disintegration of nuclei. The magnetic field is assumed to be dominated by its turbulent component namely 93% of $31.6 \mu\text{T}$ and the radius of the halo is extended to 15 kpc. Trajectories of particles have been calculated starting at random positions inside the galactic disk.

The energy spectra obtained for elemental groups are presented in Figure 17. The energies as given in [30] have been rescaled by $\delta_E = -12\%$ in order to match the all-particle spectrum (filled circles) with the average measured values (solid line). The shape of the all-particle spectrum obtained is in good agreement with the measured values. The cut-off behavior for individual element groups is softer than in the *poly-gonato* model. The steepening in the spectrum of primary protons at $\approx 10^5$ GeV is

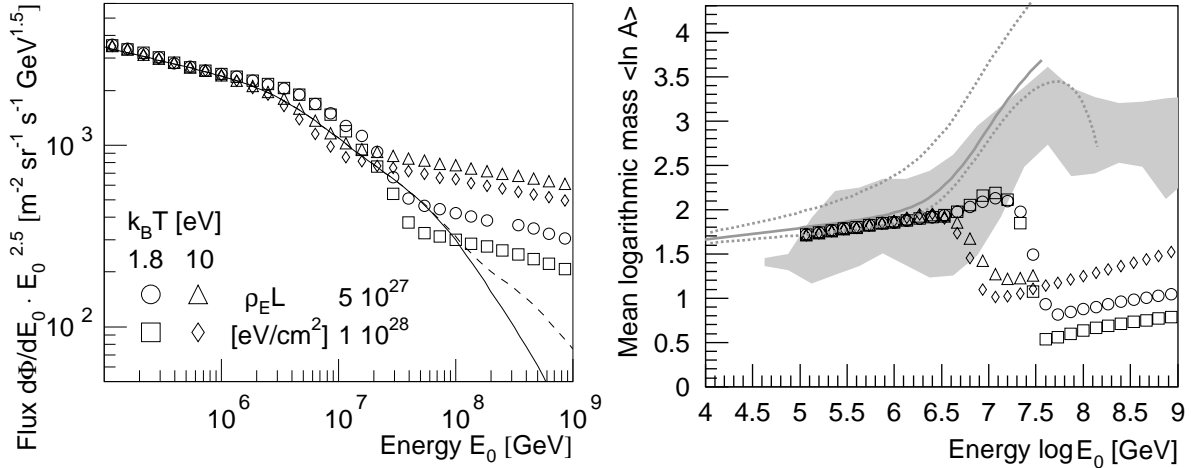


Figure 18: All-particle energy spectrum (left-hand) and mean logarithmic mass versus primary energy (right-hand) for the model by Candia et al. [32] (symbols), see also captions of Figures 4 and 6. Results for different values for the temperature T and the column density $\rho_E L$ of the photon field are shown.

due to their leakage from the Galaxy. In the region between 1 PeV and 30 PeV the *knee* in the all-particle spectrum is explained as due to photo-disintegration of nuclei and due to leakage. The photo-disintegration process delivers a large contribution of secondary protons which leads protons to become the dominant mass group above 10^8 GeV.

The predicted mean logarithmic mass, shown in Figure 4, exhibits a slight increase between 10^4 and 10^7 GeV in fair agreement with the measurements. Due to the strong contribution of secondary protons, $\langle \ln A \rangle$ decreases above 10^7 GeV in contrast to the further increase indicated by the measured values.

3.14 Photo-disintegration by optical and UV photons

Photodisintegration of cosmic-ray nuclei in dense photon fields around compact sources is also discussed in the model by Candia, Epele, and Roulet [32]. They investigate in detail the potential influence of cosmic rays passing through columns of optical and soft UV photons in the source region. They vary the column density and $k_B T$ in the Planck spectrum to study the effect on the *knee* structure. Increasing the temperature T shifts the *knee* towards lower energies whilst increasing the column density $\rho_E L$

intensifies the steepening at the *knee*. The authors conclude that a comparatively small column density of about $5 \cdot 10^{27}$ eV/cm² and a soft photon spectrum with $k_B T \approx 2$ eV describes the *knee* structure best and can, at least partly, be responsible for it.

The total energy spectrum as calculated by the authors and the appertaining mean logarithmic mass are plotted in Figure 18. The spectra at the source are assumed to be featureless extrapolations of the spectra below the *knee*. Spectra for two values of the Planck temperature $k_B T = 1.8$ eV and $k_B T = 10$ eV as well as two column densities $\rho_E L = 5 \cdot 10^{27}$ eV/cm² and $\rho_E L = 10^{28}$ eV/cm² are presented. The main mechanism of energy loss for nuclei with energy $E_0 < 10^{18}$ eV is the process of photo-disintegration. If the typical energy of the photons is in the optical range (1-10 eV), the photo-disintegration of cosmic-ray nuclei with mass A will start to be efficient at energies $E_0 \geq A \cdot 10^{15}$ eV. The appearance of the *knee* is ultimately a threshold effect.

Up to 10^7 GeV the shape of the all-particle spectrum is compatible with the average measured flux. Candia et al. remark that excessive fluxes at energies above 10^8 GeV are not troublesome since leakage from the Galaxy or different efficiencies in the acceleration mechanisms have not been considered in the present model, but

they can not be disregarded.

The mean logarithmic mass as derived from the present model is shown as function of energy in Figure 18 on the right-hand panel. Again, results taking into account different temperatures and column densities are presented. The photo-disintegration of heavy nuclei yields a strong decrease of $\langle \ln A \rangle$ above the *knee*. The extreme light composition above 10^7 GeV is significantly below the observed values.

3.15 Neutrino interactions in the galactic halo

Dova, Epele and Swain [31] link the origin of the *knee* to a "GZK-cut-off like effect" of cosmic rays interacting with massive neutrinos in the galactic halo. The average number density $n_\nu = 337/\text{cm}^3$ of standard-model neutrinos with mass $m_\nu < 1$ MeV as predicted by Big Bang cosmology is assumed to be strongly increased due to gravitational clustering in galaxies to a value $n_\nu = 1.4 \cdot 10^8/\text{cm}^3$. In addition, a magnetic dipole moment $\mu_\nu = 5.4 \pm 0.6 \cdot 10^{-6} \mu_B^3$ is adopted for massive neutrinos in order to increase the cross-section for the inelastic scattering of nucleons on the neutrino background.

Pion production with a threshold energy of $E_p = 3$ PeV is anticipated via the processes $p + \nu \rightarrow \nu + \Delta$ and $\Delta \rightarrow p + \pi$. This fixes the neutrino mass at $m_\nu = 100$ eV. The relative heavy mass is attributed to muon or tau neutrinos, but exotic objects like hypothetical dark matter particles are named as candidates as well. These particles are proposed to be inside a spheroidal galactic halo with a radius of 10 kpc. The cosmic-ray spectrum is modeled as a two component mixture ($\approx 60\%$ protons + 40% iron) with a spectral index $\gamma = -2.8$ for both components. The propagation is described by a diffusion model, taking into account the galactic magnetic field and a residence time of about $3 \cdot 10^8$ a, independent of energy.

The spectra calculated for the two groups "proton" and "iron" are given in a small energy range from 1 PeV to 30 PeV in the publication and are shown in Figure 19. The energy scale of the model has been renormalized by $\delta_E = -6\%$

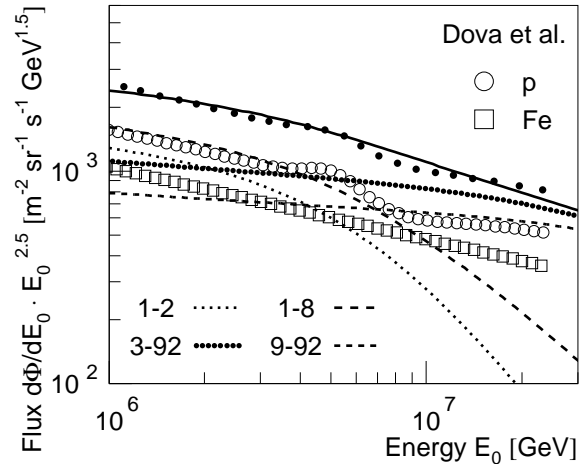


Figure 19: Energy spectra for groups of elements for the model by Dova et al. [31] (symbols) and the *poly-gonato* model (lines). The numbers indicate the range of nuclear charge used for the elemental groups, the all-particle spectrum is represented by the filled points and the solid line, respectively.

in order to fit the average all-particle flux of the measurements (solid line). In the figure the two components are compared with the *poly-gonato* model in two ways: the light component is taken as the sum of protons and helium on the one hand and as the sum for $1 \leq Z \leq 8$ on the other hand. The remaining elements up to $Z = 92$ are used for the heavy component in each case. Neither set of spectra is compatible with the calculations of Dova et al. as can be inferred from the figure. The flux of light elements above the *knee* is overestimated by the model.

The mean logarithmic mass, as calculated from the two groups is almost constant, with an average value of about 2 and a slight modulation around $10^{6.75}$ GeV, see Figure 4. At the highest energies shown, the trend towards a light mass composition is not supported by the experimental values.

3.16 New physics in the atmosphere

A completely different reason for the *knee* is discussed by Kazanas and Nicolaidis [33]. They investigate nucleon interactions hitherto unaccounted for in air showers, which transfer energy into particles not observable (or not yet

³ μ_B : Bohr magneton

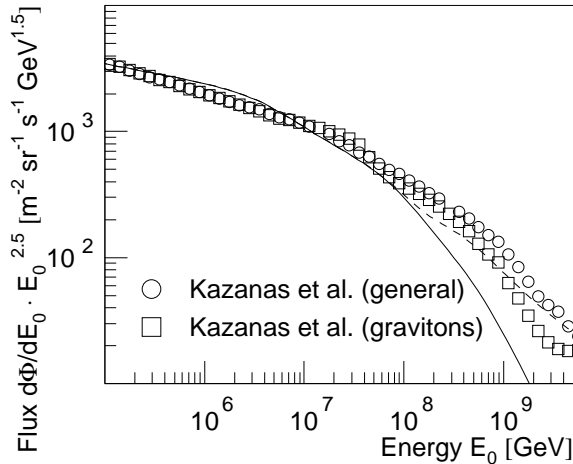


Figure 20: All-particle energy spectrum according to calculations by Kazanas & Nicolaidis for a general model [33] and for graviton production [34] (symbols). The average measured all-particle flux is shown by the solid line and above 10^8 GeV as dashed line.

observed) by air shower experiments. Candidates for new physics are supersymmetry, with the lightest supersymmetric particle carrying away the missing energy, technicolor models which produce techni-hadrons not observed by present experiments, or models in dimensions > 4 lowering the characteristic energy for gravitation to TeV energies and thus producing graviton energy carried away by "invisible" particles. Hence, the true energy of the shower inducing particle is underestimated in air shower measurements above the threshold energy. Being a threshold effect the new interaction entails a relatively sharp *knee* structure.

The conventional proton-proton total cross-section rises slowly with energy. In the model it is considered to have a constant value of $\sigma_0 = 80$ mbarn. The additional cross-section $\sigma_n(E)$ describes the proposed new type of interaction, rising strongly with energy. At energies above the threshold a fraction of protons interacts with the probability $P_n(E) = \sigma_n(E)/[\sigma_0(E) + \sigma_n(E)]$ through the new channel. Hence, more and more energy is missing in the measured components.

As primary all-particle energy spectrum the authors assume a single power law with a cut-off at an energy E_0 of the form $I = E^{-\gamma} \exp(-E/E_0)$ with $\gamma = 2.75$ and $E_0 =$

$10^{18.5}$ eV. In addition, at energies above 10^{18} eV, an extragalactic component is introduced. The all-particle spectrum above the atmosphere is modulated through the proposed new interactions. The resulting apparent spectrum, reconstructed from observations below the atmosphere is plotted in Figure 20 (circles). The model produces a spectrum with a shape similar to the average measured values, the *knee* occurs at a relative high energy above 10^7 GeV. The authors point out that the present model is very simple. Hence, some deviations between measurements and the predicted spectrum are possible.

In a second article Kazanas and Nicolaidis perform more detailed calculations of the cross-section in the case of graviton radiation [34]. As new physics in the interactions low scale gravitation is discussed. The graviton is considered to propagate not only in the usual four dimensions but in an additional compactified large dimension δ . Thus the fundamental (Planck) scale of gravity M_f is reduced to TeV energies. Any scattering process at center-of-mass energies $E > M_f$ should be accompanied by abundant graviton production, i.e. collinear bremsstrahlung of gravitons. The cross-section for graviton production in pp collisions is calculated to be $\sigma_n \propto (\sqrt{s}/M_f)^{2+\delta}$. A fit to the measured cosmic-ray spectrum yields $M_f \approx 8$ TeV and $\delta = 4$. This indicates a strong increase of the graviton production cross section as function of energy. Even at energies just above M_f , graviton radiation will be an important process.

Again, as primary spectrum a single power law has been assumed and the apparent spectrum has been calculated. It is shown in Figure 20 (squares). The spectrum is very similar to the one obtained from the more general consideration for different processes as mentioned above.

4 Discussion

All models discussed in this article are summarized in Table 2. Most of them yield similar all-particle spectra. On the other hand, the individual element spectra are quite different in some models. Some predict a very weak *knee*

Table 2: Synopsis of all models discussed.

Model	Author(s)
Source/Acceleration:	
Acceleration in SNR	Berezhko & Ksenofontov [18]
Acceleration in SNR + radio galaxies	Stanev et al. [19]
Acceleration by oblique shocks	Kobayakawa et al. [20]
Acceleration in variety of SNR	Sveshnikova [21]
Single source model	Erlykin & Wolfendale [22]
Reacceleration in the galactic wind	Völk and Zirakashvili [23]
Cannonball model	Plaga [24]
Propagation/Leakage from Galaxy:	
Minimum pathlength model	Swordy [25]
Anomalous diffusion model	Lagutin et al. [26]
Hall diffusion model	Ptuskin et al. [27], Kalmykov & Pavlov [42]
Diffusion in turbulent magnetic fields	Ogio and Kakimoto [28]
Diffusion and drift	Roulet et al [29]
Interactions with background particles:	
Diffusion model + photo-disintegration	Tkaczyk [30]
Interaction with neutrinos in galactic halo	Dova et al. [31]
Photo-disintegration (optical and UV photons)	Candia et al. [32]
New interactions in the atmosphere:	
Gravitons, SUSY, technicolor	Kazanas & Nicolaidis [33, 34]

structure, like e.g. the acceleration in cannon balls by Plaga and the anomalous diffusion described by Lagutin et al, while others obtain a steep falling flux at the *knee*, an example is the diffusion model by Kalmykov and Pavlov. The results from indirect measurements seem to favor a relative steep cut-off, see section 2.

Most models predict featureless spectra with a simple shape, however, some scenarios yield distinct features, which may have different theoretical origins. Kalmykov and Pavlov as well as Swordy consider a diffusion model and a Leaky Box model, respectively and obtain bumps at the individual *knee* positions. Consequently, they find a dip at *knee* energies in the mean logarithmic mass. The approaches by Sveshnikova (acceleration in supernova remnants) as well as Völk and Zirakashvili (reacceleration in the galactic halo) lead both to a twofold shape of the element spectra. Yet, also common features can be recognized, like the relative sharp kinks in the spectra as found by Erlykin and Wolfendale as well as by Stanev et al., both models describe acceleration in supernova remnants. The distinct shape leads in both cases to struc-

tures in the $\langle \ln A \rangle$ distribution.

The review has shown further that even similar conceptions lead to $\langle \ln A \rangle$ values covering the whole range depicted in Figure 4. As an example, acceleration in supernova remnants yields $\langle \ln A \rangle$ values at the lower edge of the experimental values (Berezhko and Ksenofontov) and also at the upper border (Kobayakawa et al.).

Unfortunately, the experiments give no conclusive energy spectra for elemental groups (Figures 1 - 3) and the mean logarithmic mass covers a relatively wide range, see Figure 4. Most astrophysical informations available from air shower measurements depend on the model used to describe the interactions in the atmosphere. Hence, an interpretation and evaluation of the data should be treated with care and it is very challenging to characterize in a quantitative way the best model to describe the origin of the *knee*.

In models which introduce new type of interactions in the atmosphere, like the one just discussed by Kazanas and Nicolaidis or the approaches by Nikolsky et al. [44] or by Petrukhin [45], the threshold for a new type of interaction

depends on the energy per nucleon. Thus, such models ultimately arrive at a mass dependent cut-off for individual element spectra. The investigations of the KASCADE group however seem to indicate a rigidity dependent cut-off for individual elements [2, 3, 4, 5, 6]. Also with the phenomenological approach of the *poly-gonato* model a rigidity dependent approach is favored [1].

In addition, the simultaneous observations of a *knee* in the electromagnetic, muonic and hadronic component by the KASCADE group [2, 46, 47] yield no major inconsistencies between the different air shower components. Therefore, a proposed new interaction would have to "hide" the energy in such a way, that no inconsistencies occur, when the measurements of different shower components are interpreted with standard particle physics. From the present experimental results new particle physics for high-energy interactions in the atmosphere seems not to be a likely explanation for the *knee*.

The interaction of cosmic rays with background particles like neutrinos or photons during their propagation causes fragmentation of heavy nuclei and the production of a large amount of secondary light nuclei, preferable protons. Models based on such an approach, like the models by Tkaczyk, Dova et al.⁴, and Candia et al. yield a very light mean logarithmic mass above *knee* energies. On the other hand, the measurements indicate an increase of $\langle \ln A \rangle$ with energy, see Figure 4, thus disfavoring interactions with background particles in the Galaxy as an explanation for the *knee*. In addition, the cross-sections for such interactions depend on the energy per nucleon. This yields a mass dependent cut-off for individual element spectra, which seems not to be favored by the measurements as mentioned above.

Numerous theories consider diffusive propagation of cosmic rays through the interstellar medium and leakage from the Galaxy as an explanation of the *knee*. The escape probability from the Galaxy in these models depends on the

⁴Dova et al give their results only for a very limited range in primary energy, but above 10^7 GeV a trend towards an extremely light mass composition can be recognized.

nuclear charge Z and a rigidity dependent cut-off behavior is obtained for the individual element spectra. These models yield a more or less strong increase of the mean logarithmic mass above the *knee* as consequence of the leakage starting with light nuclei. The change of the spectral slope at the *knee* is not very distinct in the Leaky Box model by Swordy as well as in the anomalous diffusion model by Lagutin et al. Consequently, only a modest increase of the mean logarithmic mass is obtained for energies above the *knee*, at the highest energies the predicted $\langle \ln A \rangle$ values are at the lower edge of the measurements.

Propagation of cosmic rays in the Galaxy, taking into account contributions from the regular magnetic field, a random component and anti-symmetric diffusion are described by Kalmykov and Pavlov, Ogio and Kakimoto, as well as Roulet et al. Although they consider similar scenarios, quite different energy spectra are obtained. Ogio and Kakimoto derive a very smooth transition in the *knee* region, while Kalmykov and Pavlov as well as Roulet et al. calculate a cut-off behavior similar to the measurements. The mean logarithmic mass obtained for the three models covers a wide range, and around 10^6 GeV a significantly different behavior for the individual models is found. On the other hand, they all result in similar values of $\langle \ln A \rangle \approx 3$ around $10^{7.5}$ GeV, well compatible with the measurements.

Several models attribute the *knee* to the acceleration process of cosmic rays. In the cannonball model described by Plaga, the spectral slopes change only by about $\Delta\gamma \approx 0.3$ at the *knee* and protons are the dominant nuclei even above the *knee*. Hence, the resulting mean logarithmic mass is almost a constant function of energy. It is the weakest energy dependence of all models discussed. In the single source model by Erlykin and Wolfendale heavy nuclei dominate above the *knee* and the $\langle \ln A \rangle$ values are in fair agreement with the measurements. This can also be stated for the concept of Völk and Zirakashvili [23], which allows for (re)acceleration of cosmic rays up to energies of the ankle.

Diffusive shock acceleration in supernova remnants is considered by Berezhko and Kseno-

fontov, Stanev et al., Kobayakawa et al., and Sveshnikova. Different variations of the basic theory of Fermi acceleration have been applied. Due to the finite lifetime of the shock front the maximum energy reached is limited. Typical values of $Z \cdot (0.1 - 3)$ PeV are attained. Kobayakawa et al. could increase the maximum energy reached in their calculations by the investigation of special magnetic field configurations. Sveshnikova takes into account recent supernova observations, which indicate the existence of very energetic explosions (hypernovae). In their high-velocity shock fronts particles can effectively be accelerated to high energies. The spectra obtained by the latter two scenarios are similar to the measurements and the *poly-gonato* model.

The *poly-gonato* model is purely phenomenological. The spectra obtained are most compatible with the acceleration in supernova remnants as described by Sveshnikova, especially the heavy enriched case, and diffusive propagation through the Galaxy as discussed by Kalmykov and Pavlov as well as Roulet et al. Hence, these models could be a good theoretical foundation of the phenomenological ansatz.

Most models discussed represent principle ideas, dealing with individual aspects of cosmic-ray acceleration, propagation, or interactions. Most probably, combinations of this basic processes are needed to describe nature realistically and more precise data will be necessary for a fine tuning of the free parameters in the models. These parameters have been adjusted to different sets of experimental results in the individual models. Most likely some of their predictions change, if a different set of experimental results is used.

At present, the experimental results do not allow to select a single approach as the best model to describe nature. The origin of the *knee* in the all-particle energy spectrum is not yet explained. However, within the boundaries given by the experiments, acceleration in supernova remnants and diffusive propagation through the Galaxy seem to be very attractive models to understand the origin of the *knee*.

Acknowledgment

The author would like to thank A.A. Lagutin and E. Roulet for providing numerical data for their models. Valuable discussions with J. Engler, N.N. Kalmykov, and K.-H. Kampert are acknowledged.

References

- [1] J.R. Hörandel, *Astropart. Phys.* 19 (2003) 193; preprint astro-ph/0210453.
- [2] H. Ulrich et al. (KASCADE Collaboration), *Proc. 27th Int. Cosmic Ray Con., Hamburg 1* (2001) 97
- [3] H. Ulrich et al. (KASCADE Collaboration), *Nucl. Phys. B (Proc. Suppl.)* 122 (2003) 218.
- [4] M. Roth et al. (KASCADE Collaboration), *Nucl. Phys. B (Proc. Suppl.)* 122 (2003) 317.
- [5] M. Roth et al. (KASCADE Collaboration), *Proc. 28th Int. Cosmic Ray Conf., Tsukuba 1* (2003) 139.
- [6] H. Ulrich et al. (KASCADE Collaboration), *European Physical Journal C* (2004) DOI: 10.1140/epjcd/s2004-03-1632-2; A. Haungs et al. (KASCADE Collaboration), *Acta Physica Polonica B* 35 (2004) 331; J.R. Hörandel et al. (KASCADE Collaboration), preprint aspro-ph/0311478.
- [7] D. Heck et al., Report FZKA 6019, Forschungszentrum Karlsruhe 1998 and <http://www-ik3.fzk.de/~heck/corsika/>
- [8] M. Müller et al. (KASCADE Collaboration), *Proc. 28th Int. Cosmic Ray Conf., Tsukuba 1* (2003) 101.
- [9] M. Aglietta et al., *Astroparticle Physics* 19 (2003) 329.
- [10] M. Bertaina et al., *Proc. 28th Int. Cosmic Ray Conf., Tsukuba 1* (2003) 115.
- [11] G. Navarra et al., *Proc. 28th Int. Cosmic Ray Conf., Tsukuba 1* (2003) 147.

- [12] S. Valchierotti et al., Proc. 28th Int. Cosmic Ray Conf., Tsukuba 1 (2003) 151.
- [13] D.Horns et al., Proc. 27th Int. Cosmic Ray Conf., Hamburg 1 (2001) 101.
- [14] M. Amenomori et al., Phys. Rev. D 62 (2000) 072007
- [15] M. Amenomori et al., Phys. Rev. D 62 (2000) 112002
- [16] M. Amenomori et al., Proc. 28th Int. Cosmic Ray Conf., Tsukuba 1 (2003) 107
- [17] J.R. Hörandel, J. Phys. G: Nucl. Part. Phys. 29 (2003) 2439; preprint astro-ph/0309010.
- [18] E.G. Berezhko and L.T. Ksenofontov, JETP 89, 3 (1999) 391.
- [19] T. Stanev et al., Astron. & Astroph. 274 (1993) 902.
- [20] K. Kobayakawa et al., Phys. Rev. D 66 (2002) 083004 and preprint astro-ph/0008209.
- [21] L.G. Sveshnikova, Astron. & Astroph. 409 (2003) 799; Proc. 28th Int. Cosmic Ray Conf., Tsukuba 1 (2003) 307.
- [22] A.D. Erlykin and A.W. Wolfendale, J. Phys. G: Nucl. Part. Phys. 27 (2001) 1005 and references therein.
- [23] H.J. Völk and V.N. Zirakashvili, Proc. 28th Int. Cosmic Ray Conf., Tsukuba 4 (2003) 2031.
- [24] R. Plaga, New Astronomy 7 (2002) 317.
- [25] S.P. Swordy, Proc. 24th Int. Cosmic Ray Conf., Rome 2 (1995) 697.
- [26] A.A. Lagutin et al., Nucl. Phys. B (Proc. Suppl.) 97 (2001) 267; Proc. 27th Int. Cosmic Ray Conf., Hamburg 5 (2001) 1896 and 1900; A.A. Lagutin private communication (2002).
- [27] V.S. Ptuskin et al., Astron. & Astroph. 268 (1993) 726.
- [28] S. Ogio and F. Kakimoto, Proc. 28th Int. Cosmic Ray Conf., Tsukuba 1 (2003) 315.
- [29] R. Roulet, preprint astro-ph/0310367; J. Candia et al., J. of Cosmology and Astropart. Phys. 0305 (2003) 003; J. Candia et al., JHEP 0212 (2002) 033; J. Candia et al., JHEP 0212 (2002) 032.
- [30] W. Tkaczyk, Proc. 27th Int. Cosmic Ray Conf., Hamburg 5 (2001) 1979; S. Karakula and W. Tkaczyk, Astropart. Phys. 1 (1993) 229.
- [31] M.T. Dova et al., preprint astro-ph/0112191.
- [32] J. Candia et al., Astropart. Phys. 17 (2002) 23.
- [33] D. Kazanas and A. Nicolaidis, preprint astro-ph/0103147.
- [34] D. Kazanas and A. Nicolaidis, hep-ph/0109247.
- [35] P.L. Biermann, Astron. & Astroph. 271 (1993) 649.
- [36] M. Nagano et al., J. Phys. G: Nucl. Part. Phys. 10 (1984) 1295.
- [37] M. Hamuy, preprint astro-ph/0301006.
- [38] M. Turatto et al., preprint astro-ph/0211219.
- [39] D.C. Ellison et al., Astroph. J. 487 (1997) 197.
- [40] A. Dar and A. De Rújula, preprint astro-ph/0008474, submitted to Astron. & Astroph.
- [41] V.S. Berezinsky et al., Astrophysics of Cosmic Rays, North Holland, Amsterdam 1990.
- [42] N.N. Kalmykov and A.I. Pavlov, Proc. 26th Int. Cosmic Ray Conf., Salt Lake City 4 (1999) 263.
- [43] A.M. Hillas, Proc. 16th Int. Cosmic Ray Conf., Kyoto 8 (1979) 7.

- [44] S.I. Nikolsky, Nucl. Phys. B (Proc. Suppl.) 75A (1999) 217; Proc. 27th Int. Cosmic Ray Conf., Hamburg 4 (2001) 1389; S.I. Nikolsky et al., Phys. Atomic Nuclei 63 (2000) 1799.
- [45] A.A. Petrukhin, Phys. Atomic Nucl. 66 (2003) 517.
- [46] R. Glasstetter et al. (KASCADE Collaboration), Nuclear Physics B (Proc. Suppl.) 75A (1999) 238.
- [47] J.R. Hörandel et al. (KASCADE Collaboration), Proc. 26th Int. Cosmic Ray Conf., Salt Lake City 1 (1999) 337; J.R. Hörandel et al. (KASCADE Collaboration), Proc. 27th Int. Cosmic Ray Conf., Hamburg 1 (2001) 137.